NASA TN D-1377

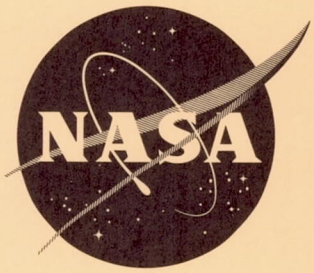

TECHNICAL NOTE

D-1377

DESCRIPTION AND PRELIMINARY CALIBRATION TESTS OF A SMALL ARC-HEATED HYPERSONIC WIND TUNNEL

By William B. Boatright, Roger B. Stewart,
and John E. Grimaud

Langley Research Center
Langley Station, Hampton, Va.

NATIONAL AERONAUTICS AND SPACE ADMINISTRATION

WASHINGTON December 1962

NATIONAL AERONAUTICS AND SPACE ADMINISTRATION

TECHNICAL NOTE D-1377

DESCRIPTION AND PRELIMINARY CALIBRATION TESTS OF A SMALL ARC-HEATED HYPERSONIC WIND TUNNEL

By William B. Boatright, Roger B. Stewart, and John E. Grimaud

SUMMARY

A description, modification history, and results of preliminary calibration experiments for a small hypersonic arc-heated wind tunnel are presented. Results obtained with different arc-heater configurations are described, and it is shown that the use of a 12,000-gauss magnetic field to rotate the arc offers distinct advantages over an arc-heater configuration with a 4,000-gauss magnetic field. These advantages are in the form of longer electrode life, less contamination, and increased steadiness of the flow. Although a higher arc voltage resulted for the same gap size for the configuration with the higher magnetic-field strength, no increase in arc-heater efficiency was produced. All arc-heater configurations were rather inefficient but this was probably, in part, due to the small throat size used and the correspondingly low air-mass-flow rates.

Pitot-pressure surveys along the center line at a stagnation pressure of 12 atmospheres and a stagnation temperature of about 3,600° K showed that the longitudinal Mach number gradient produced in the test section by the 5° half-angle nozzle was shallow. In the 3-inch-diameter test section the boundary-layer displacement was estimated to be about 0.6 inch.

Comparison of the measured total heat transferred to a small section of the wind tunnel, which included the throat, with theoretical predictions indicated that the total throat heating for the present system could be predicted reasonably well by using a laminar-boundary-layer heat-transfer theory.

INTRODUCTION

The heating of gases by electric arcs has received wide attention in recent years. Arc heating is particularly attractive because it can be used to heat gases to temperatures much higher than can be reached by utilizing chemical combustion energy or any heating process which depends on heat transfer from a solid material. An excellent review and bibliography of arc-heater development is given in reference 1. One application toward which arc-heater development has been directed is the simulation of reentry environments. A number of fairly high-powered arc heaters have been built and successfully used in materials testing to

simulate the enthalpies encountered during reentry (for example, refs. 2, 3, and 4). Reference 5 gives a discussion of the flight parameters that are of the greatest importance for proper simulation in different types of testing.

Application of arc heating to reentry simulation has been usually concerned with producing a high-enthalpy, subsonic, or supersonic flow, and this type of application has been very productive, particularly in materials testing. The applications which use arc heating to advance the capabilities of hypersonic wind tunnels for aerodynamic studies have been somewhat slower to develop but are presently beginning to become available. Their slower development has been caused by the more stringent requirements of an arc heater for a hypersonic tunnel, namely, higher operating pressure and usually less contamination than is absolutely necessary for a materials test facility. A number of arc-heated hypersonic tunnels are presently under development or construction but many problems remain to be solved before their most efficient utilization can be realized. These problems are not all necessarily concerned with arc-heater development but are concerned with many other aspects such as nozzle-flow calibration problems, throat heating, instrumentation, and so forth. Reference 6 outlines some interesting nozzle-calibration and instrumentation-development effort that has been applied to calibrating a small, fairly low-density, high-enthalpy supersonic tunnel.

This report presents a brief outline of some of the arc-heater and wind-tunnel development work which has been done at the Langley Research Center and the results of some preliminary calibration experiments. This small pilot-model facility was built for the primary purpose of working in the development and calibration problems of hypersonic arc-heated wind tunnels, and the design was strongly influenced by the requirement of utilizing as much existing equipment as possible (for example, a 900-kilowatt motor-generator and a small two-stage steam ejector).

SYMBOLS

A	cross-sectional area of nozzle
A^*	throat cross-sectional area
B	magnetic-field strength
d	nozzle diameter
h	heat-transfer coefficient
$H_{t,E}$	total enthalpy as determined by energy-balance method
$H_{t,S}$	total enthalpy as determined by sonic-throat method
I	electric current

l	length of coil
$\dot{m}$	mass flow of hot air through tunnel after arc ignition
M_∞	free-stream Mach number
N	number of turns in a coil
N_{Nu}	Nusselt number
N_{Pr}	Prandtl number
N_{Re}	Reynolds number
p_t	total pressure
p_∞	free-stream static pressure
q	heat-transfer rate
R	resistance
s	distance along surface
T_r	recovery temperature
T_t	total temperature
T_w	wall temperature
T_∞	free-stream static temperature
T'	reference temperature (defined by eq. (5))
V^*	velocity at sonic throat
V_∞	free-stream velocity
x	axial distance along nozzle
η_E	efficiency as determined by energy-balance method
η_S	efficiency as determined by sonic-throat method
ρ^*	density at sonic throat

Subscripts:

D based on diameter

s along surface

2 behind normal shock

DESCRIPTION OF WIND TUNNEL

A sketch of the wind tunnel is shown in figure 1 and a photograph showing the actual appearance of the tunnel is presented in figure 2. The arc-chamber configuration shown in figure 1 is an early configuration no longer in use. The facility consists of an arc heater which exhausts air through a water-cooled throat section 0.133 inch in diameter, a 5° half-angle conical nozzle, a 3-inch-diameter test section with window cavities, a straight-pipe diffuser, and an aftercooler to the steam ejector.

The test air, from 500-lb/sq in. storage tanks, is piped through a flow-control valve and flowmeter to the arc chamber. This same 500-lb/sq in. dry air is used to pressurize the water storage tanks (9 bottles, each 7 cubic feet) which furnish cooling water to the different components of the tunnel. The tunnel was designed so that separate measurements of the water volume flow and the water temperature rise can be taken for each electrode, the plenum chamber, the section containing the throat, and the conical nozzle.

ARC-HEATER CONFIGURATIONS

The arc-heater designs[1] which have been tested were fundamentally similar and represented a design which seemed compatible with an existing motor-generator power source which had only a 600-volt capability. Figure 3 illustrates the arc-heater configurations that have been tested. All configurations used water-cooled copper electrodes and a magnetic field to rotate the arc. Two different designs which were used for the center electrode are shown in figure 4.

Configurations 1 and 1A

A cross-sectional view of arc-heater configuration 1 is shown in figure 3(a). This configuration used a magnetic field of smaller strength than was later found to be advantageous. The 21 turns of water-cooled tubing of the coil were powered separately by a 600-ampere arc welder. For all other arc-heater configurations the coil or coils were connected in series with the direct-current arc and powered by the 900-kilowatt motor-generator. The center electrode shown in

[1]Mr. Milton A. Wallio of the Langley Electrical Engineering Branch was to a great extent responsible for the design and development of the successfully operating arc heaters used in this investigation.

figure 3(a) was not especially satisfactory since the arc location was sensitive to the magnitude of the air-mass flow and since gap sizes larger than 3/16 inch could not readily be used. Also considerable electrode erosion occurred and repairs to this type of center electrode were expensive. This configuration furnished some successful tests with arc currents as high as about 1,000 amperes, however. The circular symbols in figure 5 show the arc characteristics for this configuration at stagnation pressures up to 60 lb/sq in. The arc current was varied from about 500 to 1,000 amperes. The square symbols show the arc characteristics for configuration 1A which is a modification to configuration 1. This modification consisted of using the same center-electrode configuration, but an additional coil was added identical to that shown for configuration 2 in figure 3(b). The wide scatter in the data of figure 5 for configuration 1A is in part due to the varying electrode position used. In this case the distance, between the point where the center electrode touched the outer electrode and the center-electrode position used for the test, was varied from 5/32 to 7/32 inch, measured in a horizontal direction. (This dimension does not represent the actual arc gap.)

Configuration 2

Figure 3(b) shows a cross-sectional view of arc-heater configuration 2. This configuration furnished a large number of successful tests, and the arc characteristics for this configuration at a stagnation pressure of approximately 180 lb/sq in. are denoted by the diamond symbols in figure 5. As figure 5 shows, it was possible to operate this configuration at higher power levels than configuration 1. The doughnut-shaped center electrode (fig. 4(a)) was also easily and cheaply replaced whenever a burnout occurred. The tests with this configuration were conducted with the center electrode spaced 9/16 inch (in a horizontal direction) from the point where the center electrode would touch the outer electrode.

Figure 6 shows a vector diagram of the magnetic-field strength in the region of the arc for configuration 2. These magnetic-field strengths were calculated for the case which consisted of a current of 1,600 amperes passing through the small coil and 800 amperes through each 32-turn winding of the large coil. Since all metal parts of the arc chamber were made of 347 stainless steel or copper, there should be negligible distortion of the flux lines due to the arc pressure case. Figure 6 shows that the magnetic-field strengths in the region of the arc were in the neighborhood of 4,000 gauss for configuration 2.

Configuration 3

A cross-sectional view of arc-heater configuration 3 is shown in figure 3(c), and the corresponding arc characteristics for this configuration operating at a stagnation pressure of about 180 lb/sq in. are denoted by the triangular symbols in figure 5. The approximate formula

$$B = \frac{0.2\pi NI}{2.54\sqrt{R^2 + (l/2)^2}} \qquad (1)$$

gives the field strength at the center of a solenoid when R and l are expressed in inches. With use of this formula the magnetic-field strength was calculated to be about 12,000 gauss for tests with an arc current of 1,200 amperes. Measurements with a gauss meter confirmed this field-strength intensity. The electrical circuit and the coil data which were used with configuration 3 are shown in figure 7. Also shown in figure 7 are some measurements made at various points in the electrical circuit during a typical test at a stagnation pressure of about 180 lb/sq in. Figure 5 shows that with configuration 3 (triangular symbols) more power could be put into the arc than with configuration 2 (diamond symbols) and that the voltage did not tend to decrease with increasing current as it did for configuration 2. These data for configurations 2 and 3 were taken at about the same stagnation pressure of 180 lb/sq in. Since the coils were in series with the arc for both configurations 2 and 3, the primary reason for the flatter voltage-current characteristic with configuration 3 is the fact that the increase in field strength with increase in current was greater for configuration 3 than for configuration 2. The stronger magnetic field therefore increases the effective voltage gradient between the electrodes at a greater rate with the same increase in current. Although the anode for configuration 3 was 1/4 inch larger in diameter than that for configuration 2, the inner electrode was also increased in size so that the radial geometric gap was the same for both configurations 2 and 3. Also, the voltage drop across the ballast resistance plus the voltage drop across the coil was approximately equal to the voltage drop across the arc for both configurations 2 and 3 in this series of tests at a stagnation pressure of approximately 180 lb/sq in. The ballast resistance was made less for configuration 2 than for configuration 3 to allow for the increased resistance of the larger coil. It can be shown by a simple derivation that, when the ballast resistance is equal to the arc resistance, then minimum power fluctuations will occur for small fluctuations in the arc gap.

INPUT-POWER STEADINESS

It might be conjectured that the large inductive reactance of the coil would tend to dampen any high-frequency oscillations of the arc current and that the pure ballast resistance would tend to dampen low-frequency oscillations. The voltage-current records for some typical tests are shown in figure 8. The records shown in figures 8(a) and 8(b) were taken with a type of instrument which had a slow response (about 0.3 second). A comparison of figures 8(a) and 8(b) shows that there was a great improvement in the steadiness of the power input to the arc for configuration 3 with its high magnetic-field strength as compared with configuration 2. (This result is evident even though the scale factor is different in figs. 8(a) and 8(b).) The results of operation at high magnetic-field strengths (up to 12,000 gauss) supported the reported data on diffuse arcs presented in reference 7. Figure 8(c) shows an oscillograph record of the voltage and amperage across the arc for configuration 3 with its 12,000-gauss field strength. The galvanometer element in this instrument was capable of a response rate of about 5,000 cycles per second. Figure 8(c) shows that there is about a

100-volt fluctuation in the voltage trace whereas the current trace is very steady.

A series of tests were made with configuration 3 at stagnation pressures up to 435 lb/sq in. For these tests, the arc voltage increased with pressure to a value of 355, and it was necessary to decrease the ballast resistance in series with the arc in order to stay within the 600-volt limitation of the motor-generator power supply. The voltage-current traces were not as smooth as those shown in figure 8(b) but were considerably smoother than those shown in figure 8(a).

ARC-HEATER PERFORMANCE

The two stagnation properties which are usually measured to determine the stagnation conditions in an arc heater are pressure and enthalpy. These conditions, of course, fix all other stagnation properties if the flow is in equilibrium. For the low airflow velocity and correspondingly long dwell time in the arc heater of this small pilot-model facility with its small throat size, it was assumed that the flow was in equilibrium before reaching the throat section. Therefore, the measurement of pressure and enthalpy should determine the state of the gas. A pressure tap between the sections comprising the outer electrode and the plenum chamber was used for measuring the stagnation pressure.

The enthalpy was usually determined by two different methods. The first method was the commonly used energy-balance method which consists of measuring the voltage and amperage across the arc to determine the power supplied to the arc, and then subtracting from this power input, the power losses to the cooling water. The power losses to the cooling water were evaluated by measuring the water flow rates by means of turbine-type flow meters, and the water temperature rise was measured by thermocouples in the outlet lines. The water flow rates and temperature rises were recorded on self-balancing recording potentiometers. In some cases, water temperature was also measured by using a recording oscillograph.

The second method for determining the enthalpy is based on the assumption of sonic flow in the throat and the assumption that the flow remains in equilibrium up to the throat section. If the effective throat area is known, the total average enthalpy can be obtained from a measurement of the mass flow of air through the heater and the stagnation pressure in the heater. The technique for determining the enthalpy in this manner is illustrated by writing the continuity equation in the following form:

$$\frac{\dot{m}}{A^*} = \rho^* V^* \tag{2}$$

For any set of stagnation conditions, ρ^* and V^* can be calculated by using tables of thermodynamic properties of air or a Mollier diagram for equilibrium air. Thus, curves of $\dot{m}/A^*$ for various stagnation enthalpies and pressures can be constructed, as for example, on page 70 of reference 8. Experimental measurements

of $\dot{m}$ and p_t and curves of this type will therefore determine the enthalpy of the air. Alternately, curves of this type can be used to determine an analytical expression for $H_{t,s}$ as a function of $\dot{m}$, p_t, and A^*. (See ref. 9.) One weakness in determining enthalpy by using this technique is the assumption that the geometric throat area is equal to the effective throat area. For small throat sizes, this assumption can introduce a serious error.

Bar graphs illustrating the performance of various arc-heater configurations for some typical tests as given by the energy-balance method are shown in figure 9. Figures 9(a), 9(b), and 9(c) illustrate the performance of configurations 1A, 2, and 3, respectively. The stagnation pressure was approximately 12 atmospheres for this series of tests. The total enthalpy of the air at the throat location as determined by each method is also shown in figures 9(a), 9(b), and 9(c). All configurations proved rather inefficient. Figure 9(c) shows that, although it was possible to get more power into the arc for configuration 3 as compared to configuration 2 (fig. 9(b)), there was a decrease in efficiency and the power actually obtained in the air was no greater. This result was disappointing since it was expected that operating at higher voltage across the arc gap would increase the efficiency. Although configuration 3 did not operate as efficiently, other considerations to be discussed subsequently made it a more desirable configuration than any of the other configurations which were tested.

The low efficiency of these arc-heater configurations is in part due to the small throat size used. References 9 and 10 indicate that increases in efficiency are obtained with increasing airflow rate through the heater. In fact, figures 9(c) and 9(d) show a slight increase in efficiency with increasing stagnation pressure if the increased losses to the throat section at higher pressures are discounted. The efficiency in this case would be the power to the air plus the throat loss divided by the input power. The cross-hatched portions of the bar graphs in figures 9(d), 9(e), and 9(f) represent the calculated power which is in the air at a location just upstream of the throat section if it is assumed that radiant-heat losses to the throat section are negligible. The slight increase in efficiency produced by increasing the stagnation pressure from about 12 atmospheres to about 20 atmospheres (figs. 9(c) and 9(d)) results in spite of the fact that the aerodynamic convective heating in the arc chamber is greater at a higher pressure.

In an attempt to improve the efficiency of arc-heater configuration 3, the doughnut-shaped center electrode (fig. 4(a)) was replaced by the cup-shaped center electrode (fig. 4(b)). Configuration 3 with a cup-shaped center electrode will be referred to as configuration 3A. The relative performance of configurations 3 and 3A can be compared in figures 9(d) and 9(e). Based on the energy-balance method, these tests at a stagnation pressure of about 20 atmospheres show a slight increase in efficiency is produced by changing from configuration 3 to configuration 3A. The converse is true, based on the equilibrium-sonic-flow method.

Figure 9(f) shows the results of a typical test at a stagnation pressure approaching 30 atmospheres. The anode and cathode losses still are not significantly increased because of the higher pressure; however, according to the energy-balance method there is little useful power in the air downstream of the throat section because of the increased losses in the plenum chamber and the throat section. The enthalpy as determined by the sonic-flow method shows an increase in

efficiency at this higher operating pressure. Whether this discrepancy is due to a violation of the assumptions within the sonic-flow technique or simply inadequate experimental accuracy was not determined. It should be noted that, with use of the energy-balance method at low arc-heater efficiencies, a small percentage error in determining the losses to the cooling water can cause a large percentage error in the power to the air. Since the enthalpy is the power to the air divided by the air mass flow, a large error in enthalpy determination results.

TEST-SECTION CALIBRATION

Pitot Measurements

Initial test-section calibration measurements were made with a flat-faced water-cooled pitot tube, 1/2 inch in diameter. The pitot tube for the longitudinal survey along the tunnel axis was supported by a spider in the support box (see fig. 1) and extended up through the straight-pipe diffuser to the test section. The pitot tube was designed by using stock tubing with three concentric passages such that the pressure signal was carried by the inside passage, whereas the outer two passages conveyed the cooling water. Figure 10(a) shows the results obtained with this pitot tube for the arc-heater configurations with the 4,000- and 12,000-gauss fields (square and diamond symbols). The tunnel was operated at a stagnation pressure of 12 atmospheres and a calculated stagnation temperature of 3,600° K for these tests. As might be expected there was essentially no effect of different arc-heater configurations on the pitot-pressure measurements. A lateral survey made with a pitot tube 3/8 inch in diameter and side-mounted from the window cavity also showed no pronounced effect of the different arc heaters. (See fig. 10(b).) It was suspected from the start of these pitot surveys that the tube was too large for the tunnel so a great deal of effort went into attempting to fabricate a pitot probe which was smaller in diameter and yet one which would survive the high temperatures. A probe which was cooled by water injection (and therefore needed only one water passage) was built and tested but there were many difficulties connected with testing this probe. One difficulty was that the cooling water would freeze on the nose of the probe with airflow through the tunnel before the arc was ignited. Thus, a large ice cap would form on the nose in a very few seconds. Eventually a 5/16-inch-diameter probe made completely of copper was built and used to obtain the data shown by the circular symbols in figure 10. This probe was fabricated with three concentric passages similar to the 1/2-inch-diameter probe but the wall thickness of the three concentric tubes was made thinner and the nose of the probe was slightly rounded at the edges. From the results of the tests with the two probe sizes it is evident that the tunnel flow must have been separated from the nozzle walls for the tests with the 1/2-inch-diameter probe.

Figure 11 shows a series of pictures which were obtained from movies of the different probes during their tests. The movies were taken at 24 frames per second. It can be seen in figure 11(a) that the flow upstream of the 1/2-inch-diameter probe appears much the same as the flow in the picture on the left of figure 11(b) with the 5/16-inch-diameter probe. The picture on the left of figure 11(b) was taken during the first few seconds after arc ignition and before the flow in the test section was fully established. The picture on the right of

figure 11(b) was taken after the flow was established. Movies of the test with the small probe showed that a shock from the juncture of the conical nozzle and the cylindrical test section was formed after the flow was established. This shock failed to appear in the movies of the tests with the 1/2-inch-diameter probe, and the luminous core was noticeably smaller. The lateral pitot survey with the 5/16-inch-diameter probe (fig. 10(b)) indicates a rise in pitot pressure at a point about 0.3 inch from the tunnel center line. The movies indicated that this rise in pressure could be attributed to the shock from the cone-cylinder juncture. Outboard of this point where the rise in pressure occurs, in the region where the pitot-pressure measurements again start decreasing, the pitot measurements are not to be correlated with the Mach number scales to the right of figure 10 because of change in total pressure within the boundary layer. The pressures associated with the longitudinal survey and the pressures near the tunnel center line of the lateral survey can be matched with the Mach number scales, and it is seen from figure 10(a) (small probe) that between 1 and 4 inches downstream of the cone-cylinder juncture, the longitudinal Mach number gradient is shallow for this 5° half-angle conical nozzle. Experimental determination of whether the flow is in equilibrium or partially frozen in the nozzle is beyond the scope of this report.

It is interesting to note that, at the cone-cylinder juncture where the geometric area ratio A/A^* is 509, the pitot-pressure results indicate a Mach number of about 9.1 for frozen flow and 6.4 for equilibrium flow. One-dimensional calculations of the expected Mach number at this area ratio indicate that a Mach number of 7.85 should be obtained with equilibrium flow in the nozzle and with no tunnel boundary layer. Alternately, the area ratio which would produce a Mach number of 6.4 with equilibrium flow in the nozzle is 187. This area ratio as determined by a one-dimensional analysis and a pitot-pressure measurement indicates that the boundary-layer-displacement thickness is approximately 0.6 inch at the cone-cylinder juncture where the nozzle diameter is 3 inches. A similar analysis for frozen flow would indicate nearly the same effective area since pitot pressures are fairly insensitive to whether the flow is frozen or in equilibrium.

Flow Steadiness and Contamination

As previously mentioned, no increase in efficiency was obtained in changing from arc-heater configuration 2 to configuration 3. However, large increases in electrode life made configuration 3 more desirable. For configuration 2 with its 4,000-gauss magnetic-field strength, the center electrode eroded about 0.010 inch on its outside diameter during a 1-minute test when the center electrode was made of electrolytic tough pitch copper. An erosion of about 0.005 inch occurred when oxygen-free copper was used for the center electrode. A test which was of 2-second duration showed that over 50 percent of this erosion occurred during these 2 seconds. For a 1-minute test with arc-heater configuration 3, the erosion of the center electrode was less than 0.001 inch on the diameter. Corresponding contamination estimates for the tests with configuration 2 were about 1.5 percent and less than 0.2 percent for configuration 3. Figure 12 shows a series of consecutive frames from a high-speed movie (200 frames per second) of the luminous gas cap at the nose of the 1/2-inch-diameter water-cooled pitot tube. Figure 12(a) shows the results for configuration 2 with its 4,000-gauss field, and figure 12(b) shows the results for configuration 3 with its 12,000-gauss field. Both series of

pictures were made with the same camera exposure so the decrease in the luminosity shown in figure 12(b) compared with figure 12(a) actually existed. In fact, it was noticeable to the naked eye. It might be expected that the greater luminosity which occurred for configuration 2 is associated with its greater stream contamination by vaporized copper.

It can also be seen that the movies shown in figure 12(b) have less variation in luminosity than those shown in figure 12(a). This result indicated that the flow with arc-heater configuration 3 might be steadier.

NOZZLE-THROAT HEATING

The throat survival problem appears to be one of the most critical problems confronting the development of high-enthalpy hypersonic facilities. The survival capabilities of water-cooled throat sections are usually limited by the film coefficient between the throat liner and the water. Of course, increasing the water velocity increases this heat-transfer coefficient and increases the performance capabilities of the throat.

A photograph of a portion of one of the throat sections used with the small arc tunnel of this report is shown in figure 13, and a cross-sectional view of this splined copper liner is shown in figure 14(a). Figure 14(b) shows an alternate design for a throat liner which is made of beryllium copper. It was not possible to make an experimental comparison of the survival capabilities of the two types of throat designs since the arc heater has not yet been tested at sufficiently high stagnation pressures and temperatures to threaten the survival of either of these types of throat designs. After a period of over 100 tests, the splined copper liner broke during a disassembly operation, whereas the liner shown in figure 14(b) is still in use. The design philosophy for using the splined copper liner was to use splines on the water side of the liner to increase the strength of the liner and to increase the surface area in contact with the coolant. Splines were not used in the beryllium copper liner, and a portion of the high thermal conductivity of pure copper was sacrificed for the greatly increased strength of the beryllium copper.

Cooling water was supplied to both throat sections at pressures up to 400 lb/sq in. Iron-constantan thermocouples were used on the outlet water lines to indicate the temperature rise of the water through the throat section. Signals from these thermocouples were automatically recorded on self-balancing potentiometers. The water flow rates were measured by using turbine-type flow meters, and the direct-current signals from the indicators used with these flow meters were also automatically recorded on self-balancing potentiometers. The total-heat loss to the cooling water during its passage through the throat section could thus be measured. These measurements will be compared with theoretical predictions of throat heat transfer in this section of the report.

In order to calculate the heat-transfer coefficients at stations along the throat section, it is first necessary to calculate the inviscid flow properties at arbitrarily chosen stations along the axis of the throat section. The calculation was performed by using the given values of stagnation pressure and enthalpy

and the transport properties for high-temperature air which are presented in reference 11. With the assumption of equilibrium flow through the throat section, the calculated values of stream temperature, pressure, and velocity can be used to obtain laminar, compressible heat-transfer coefficients at each station.

Several empirical equations exist for estimating heat transfer at a series of stations along the throat section. It will be shown subsequently that two of the equations used, which assume laminar flow through the throat, give good agreement with measured values of the total-heat input to the cooling water. An equation presented in reference 12, which assumes turbulent nozzle flow, predicts values of the total-heat input to the cooling water as much as 3 times higher than the measured values.

The expression for the laminar, compressible heat-transfer coefficient has been derived in references 13 and 14 from the Pohlhausen expression which is:

$$N_{Nu} = 0.332 N_{Re,s}^{0.5} N_{Pr}^{0.33} \tag{3}$$

It is shown in detail in reference 14 that by using equation (3) the heat-transfer coefficient can be expressed as:

$$h = \frac{0.00963(p_\infty V_\infty)^{0.5}}{T'^{0.04} s^{0.5}} \quad \text{Btu/ft}^2\text{-hr-}^\circ\text{F} \tag{4}$$

where

$$T' = 0.5(T_w + T_\infty) + 0.22(T_r - T_\infty) \tag{5}$$

$$T_r = T_\infty + r(T_t - T_\infty) \tag{6}$$

For sufficiently small steps, a continuous curve of the heat-transfer coefficient can be plotted and a heating-rate profile obtained from:

$$q/A = h(T_r - T_w) \tag{7}$$

Such a curve, labeled as reference 14, is given in figure 15.

Another equation for calculating stepwise heat-transfer coefficients in throat entrance regions is given in reference 15 as follows:

$$N_{Nu,D} = 3.65 + \frac{0.0668(d/x)N_{Re,D}N_{Pr}}{1 + 0.04(d/x)N_{Re,D}N_{Pr}^{0.667}} \tag{8}$$

In this equation the Prandtl number, viscosity, and conductivity are introduced at a reference temperature defined as:

$$T' = 0.5(T_w + T_\infty)$$

The calculated values of q/A with use of equation (8) are also presented in figure 15 (labeled ref. 15). Mechanical integration of calculated heating-rate profiles, such as are shown in figure 15, were used to obtain the theoretical curves shown in figure 16. Figure 16 compares the theoretical predictions of references 14 and 15 with experimental measurements of the total-heat loss to the complete throat section. Within the rather poor experimental accuracy of the measurements, the agreement is good. However, the data are sufficiently accurate to conclude that measurements of the total-heat input are in agreement with the approximate methods of references 14 and 15.

CONCLUSIONS

Operational experience and preliminary calibration experiments with a small hypersonic arc-heated tunnel have indicated the following general conclusions:

1. The different arc-heater designs which were tested showed that increasing the magnetic-field strength (which is used to produce arc rotation) from about 4,000 gauss to about 12,000 gauss greatly decreased the electrode erosion and corresponding contamination of the airstream. No increase in efficiency was obtained, although for the same arc gap the arc voltage was greatly increased.

2. The variation of the voltage and amperage across the arc with time was much smoother for the arc-heater configuration with the high magnetic-field strength, and high-speed movies of stagnated air in the test section indicated less fluctuation in luminosity for the arc-heater configuration with the high magnetic-field strength.

3. All arc-heater configurations tested were rather inefficient but this was probably, to a great extent, associated with the small throat size and correspondingly low air-mass-flow rates which resulted. Increasing stagnation pressure from 12 to about 20 atmospheres increased the efficiency of the arc heater with the 12,000-gauss magnetic-field strength.

4. The 5° half-angle nozzle when tested at a stagnation pressure of 12 atmospheres and a stagnation temperature of about $3,600^\circ$ K produced a test Mach number of about 6.4 with the assumption of equilibrium flow. The longitudinal Mach number gradient was shallow in the region from about $\frac{1}{3}$ to $1\frac{1}{3}$ nozzle diameters downstream of the juncture of the conical nozzle and the cylindrical test section.

5. Measurements of the total heat transferred to a small section of the tunnel which included the throat indicated that available laminar heat-transfer theories can be used to predict the total heating to this section with reasonable accuracy.

Langley Research Center,
National Aeronautics and Space Administration,
Langley Station, Hampton, Va., August 2, 1962.

REFERENCES

1. John, Richard R., and Bade, William L.: Recent Advances in Electric Arc Plasma Generation Technology. ARS Jour., vol. 31, no. 1, Jan. 1961, pp. 4-17.

2. Rose, P., Powers, W., and Hritzay, D.: The Large High Pressure Arc Plasma Generator: A Facility for Simulating Missile and Satellite Re-Entry. Res. Rep. 56 (AFBMD-TR-59-6), Avco-Everett Res. Lab., June 1959.

3. Anon.: Air Arc Simulates Re-Entry Problems. Aviation Week, vol. 69, no. 2, July 14, 1958, pp. 71-73.

4. Kotanchik, Joseph N.: The Use of High-Intensity Arcs in Arc-Image Furnaces and Electric Arc-Powered Jets. High Intensity Arc Symposium, Stanley D. Mark, Jr., ed., The Carborundum Co., c.1958, pp. 14-28.

5. Georgiev, Steven: The Relative Merits of Various Test Facilities With Regard to Simulation of Hypersonic Ablation Phenomena. Proc. Nat. Symposium on Hypervelocity Techniques, Inst. Aero. Sci., Oct. 1960, pp. 162-174.

6. Christensen, Daphne, and Buhler, Rolf D.: Arc Jet Tunnel Development and Calibration for Parabolic Re-Entry Simulation. IFR011-1872 (Contract DA-04-495-506-ORD-1872), Plasmadyne Corp. (Santa Ana, Calif.), June 3, 1961.

7. Mayo, Robert F., and Davis, Don D., Jr.: Magnetically Diffused Radial Electric-Arc Air Heater Employing Water-Cooled Copper Electrodes. [Preprint] 2453-62, American Rocket Soc., Mar. 1962.

8. Yoshikawa, Kenneth K., and Katzen, Elliot D.: Charts for Air-Flow Properties in Equilibrium and Frozen Flows in Hypervelocity Nozzles. NASA TN D-693, 1961.

9. Shepard, Charles E., and Winovich, Warren: Electric-Arc Jets for Producing Gas Streams With Negligible Contamination. [Preprint] 61-WA-247, ASME, Nov.-Dec. 1961.

10. Eschenbach, R. C., Skinner, G. M., and Arc Laboratory Staff: Development of Stable, High Power, High Pressure Arc Air Heaters for a Hypersonic Wind Tunnel. WADD Tech. Rep. 61-100, U.S. Air Force, July 1961.

11. Hansen, C. Frederick: Approximations for the Thermodynamic and Transport Properties of High-Temperature Air. NASA TR R-50, 1959. (Supersedes NACA TN 4150.)

12. Bartz, D. R.: A Simple Equation for Rapid Estimation of Rocket Nozzle-Convective Heat Transfer Coefficients. Jet Propulsion (Tech. Notes), vol. 27, no. 1, Jan. 1957, pp. 49-51.

13. Fluid Motion Panel of the Aeronautical Research Committee and Others: Modern Developments in Fluid Dynamics. Vols. I and II, S. Goldstein, ed., The Clarendon Press (Oxford), 1938.

14. Harms, Richard J., Schmidt, Craig M., Hanawalt, Arnold J., and Schmitt, Durwin A.: A Manual for Determining Aerodynamic Heating of High-Speed Aircraft - Volume I. Rep. No. 7006-3352-001, Bell Aircraft Corp., June 1959.

15. Eckert, E. R. G. (With Pt. A and Appendix by Robert M. Drake, Jr.): Heat and Mass Transfer. Second ed. of Introduction to the Transfer of Heat and Mass, McGraw-Hill Book Co., Inc., 1959.

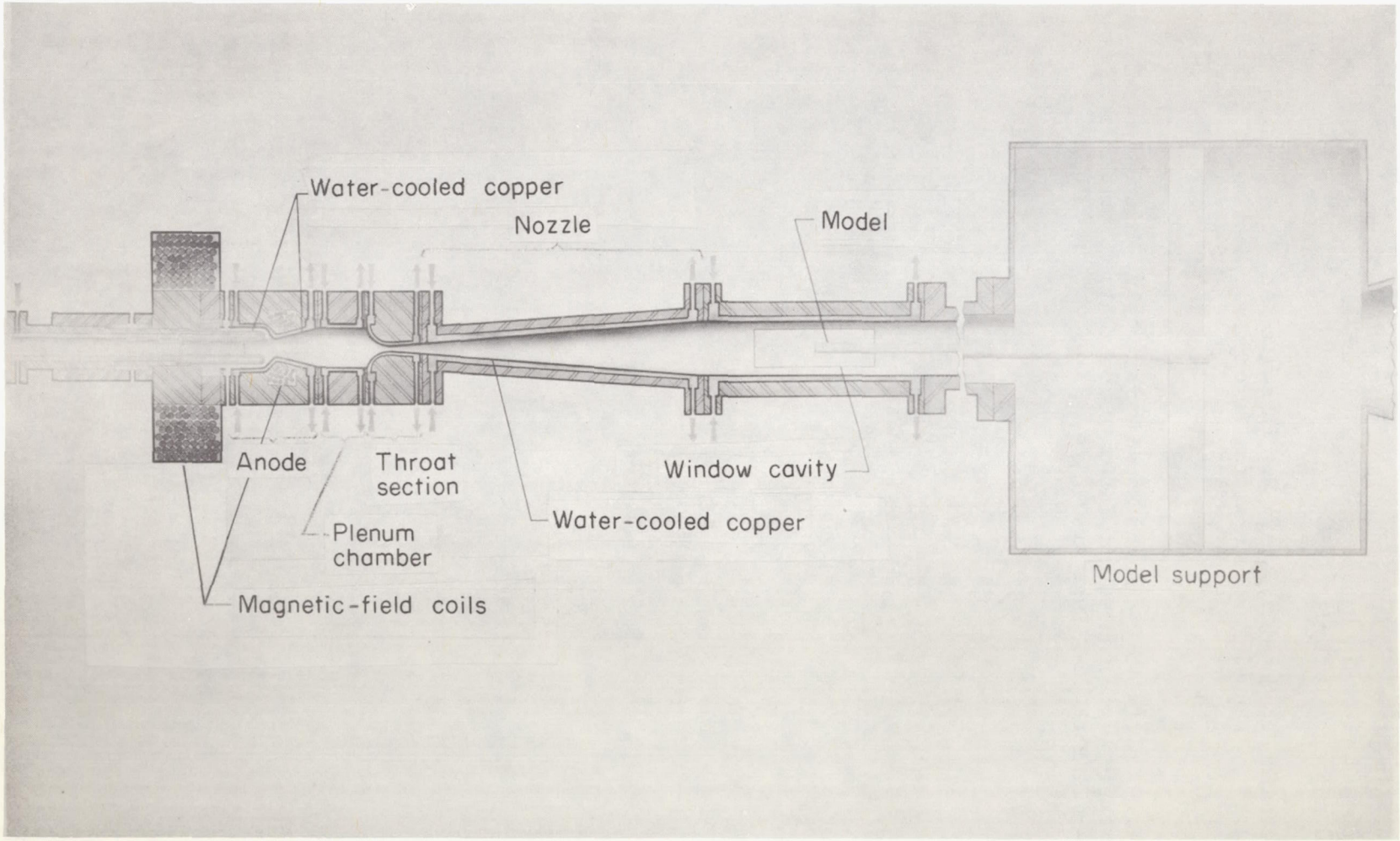

Figure 1.- Schematic drawing of arc-heated tunnel.

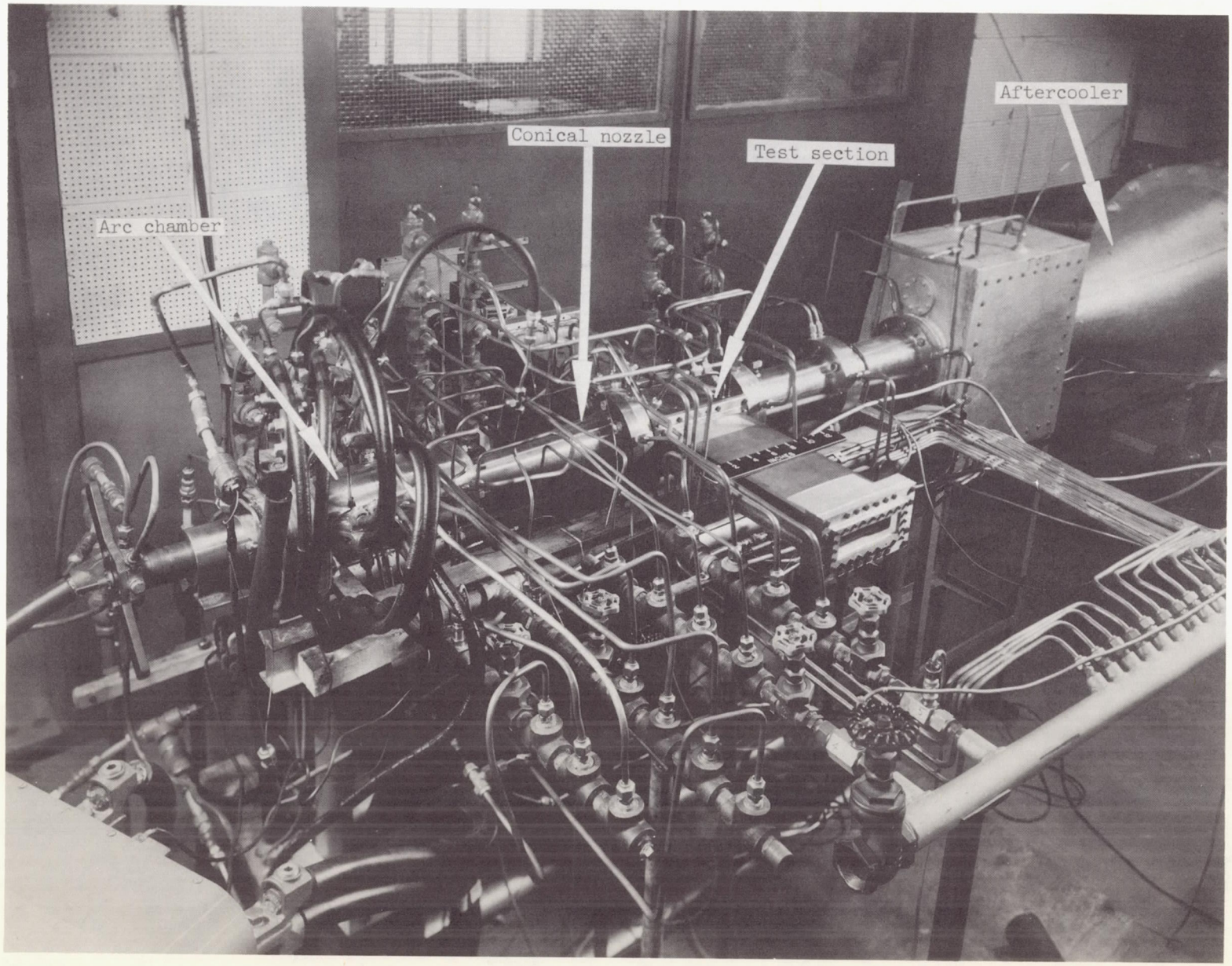

Figure 2.- Photograph of arc-heated tunnel (arc-heater configuration 2). L-60-7288.1

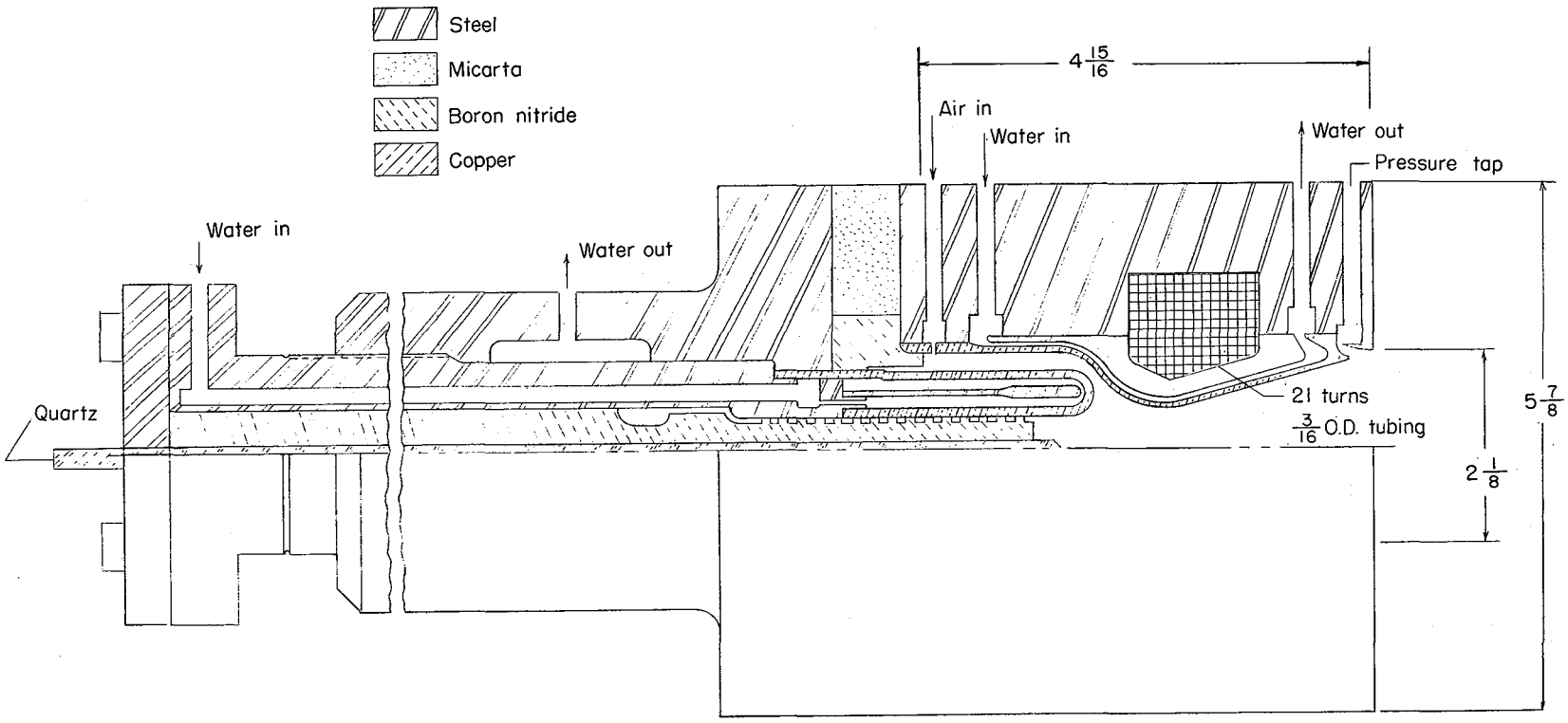

(a) Configuration 1.

Figure 3.- Section view of arc-heater configurations. (All dimensions are in inches.)

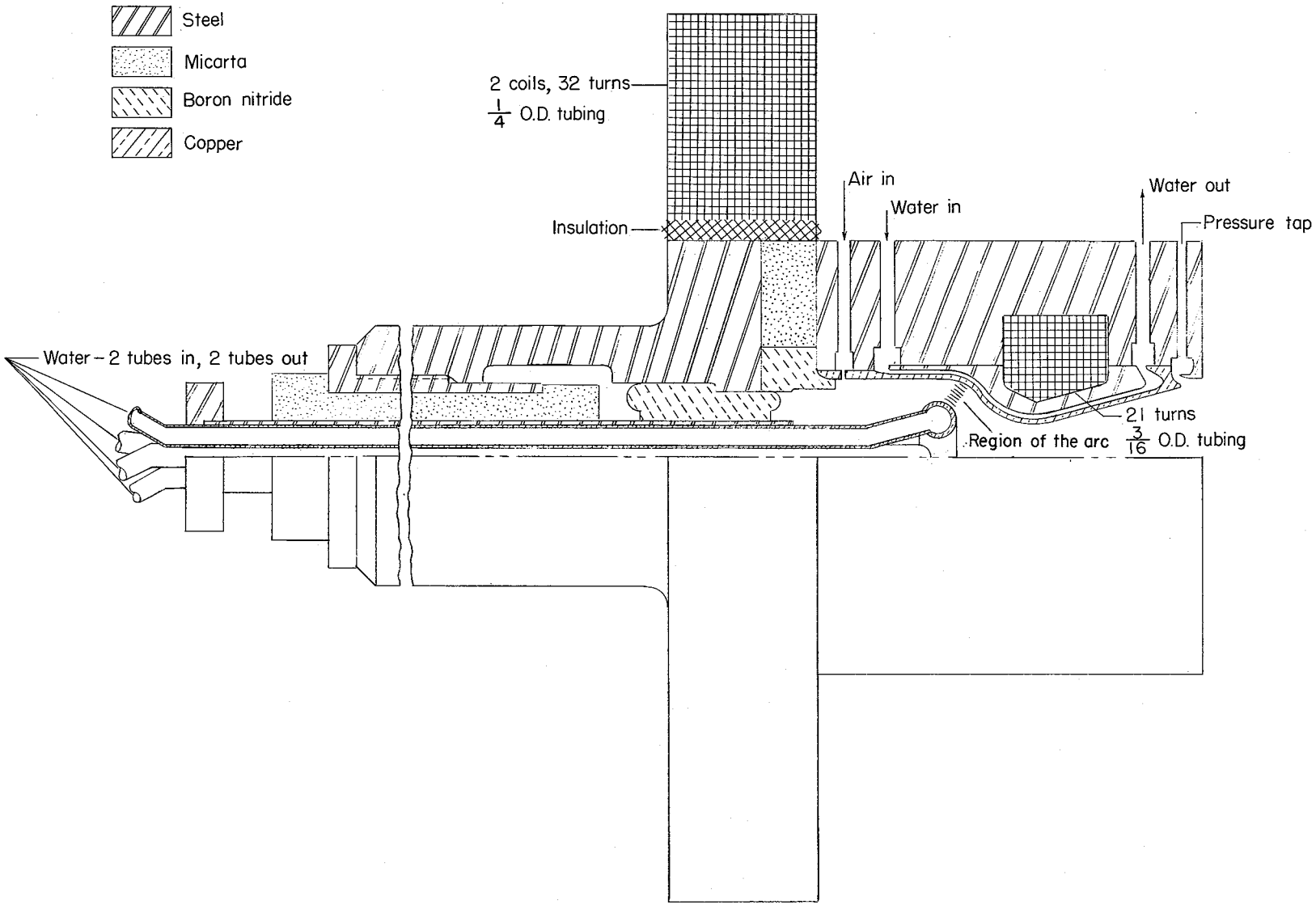

(b) Configuration 2.

Figure 3.- Continued.

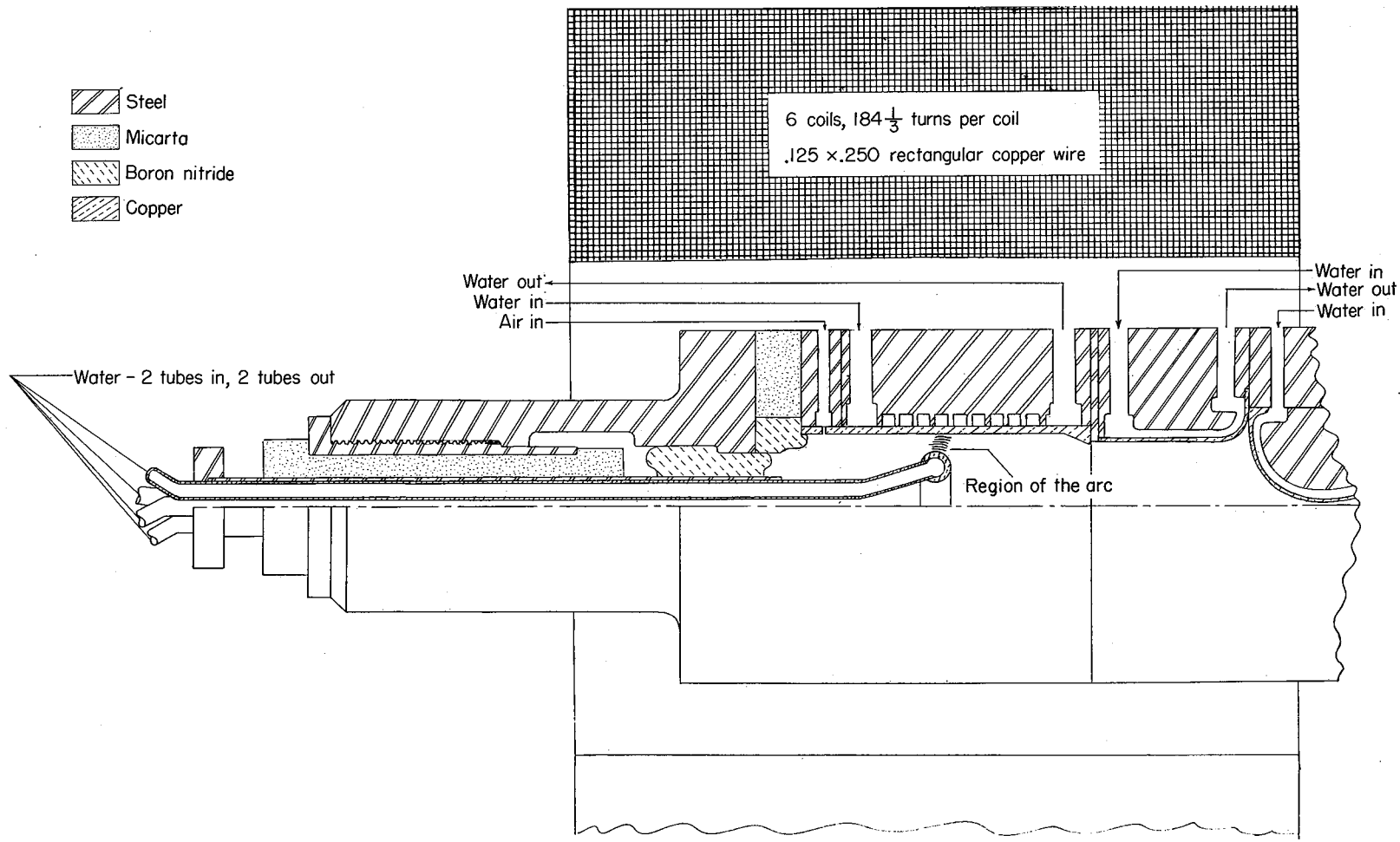

(c) Configuration 3.

Figure 3.- Concluded.

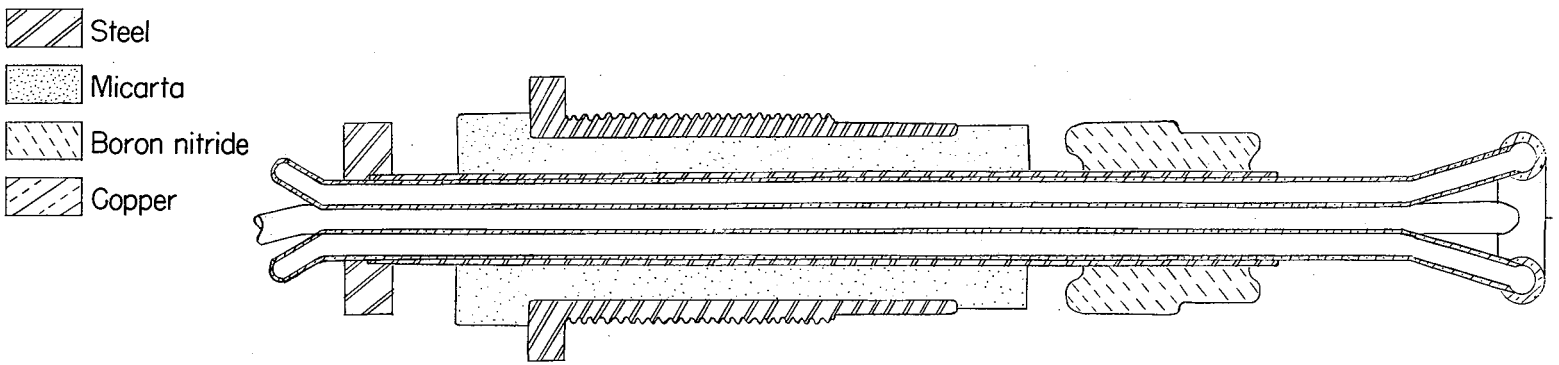

(a) Doughnut-shaped electrode.

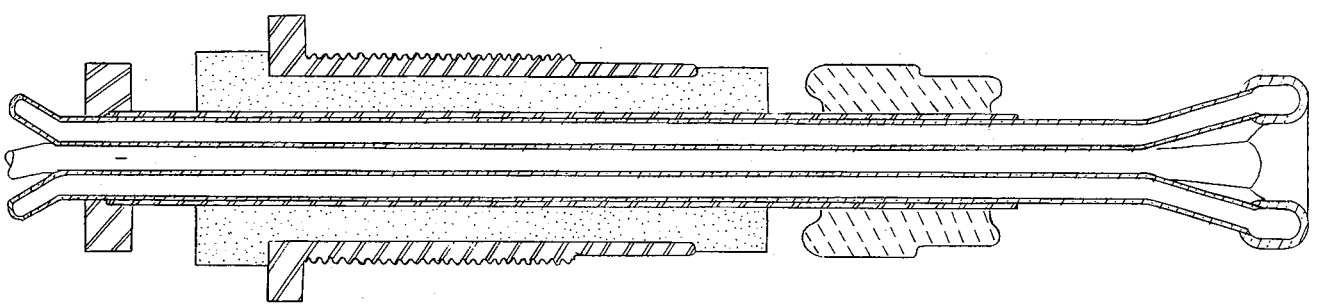

(b) Cup-shaped electrode.

Figure 4.- Cross-sectional view of center-electrode configurations.

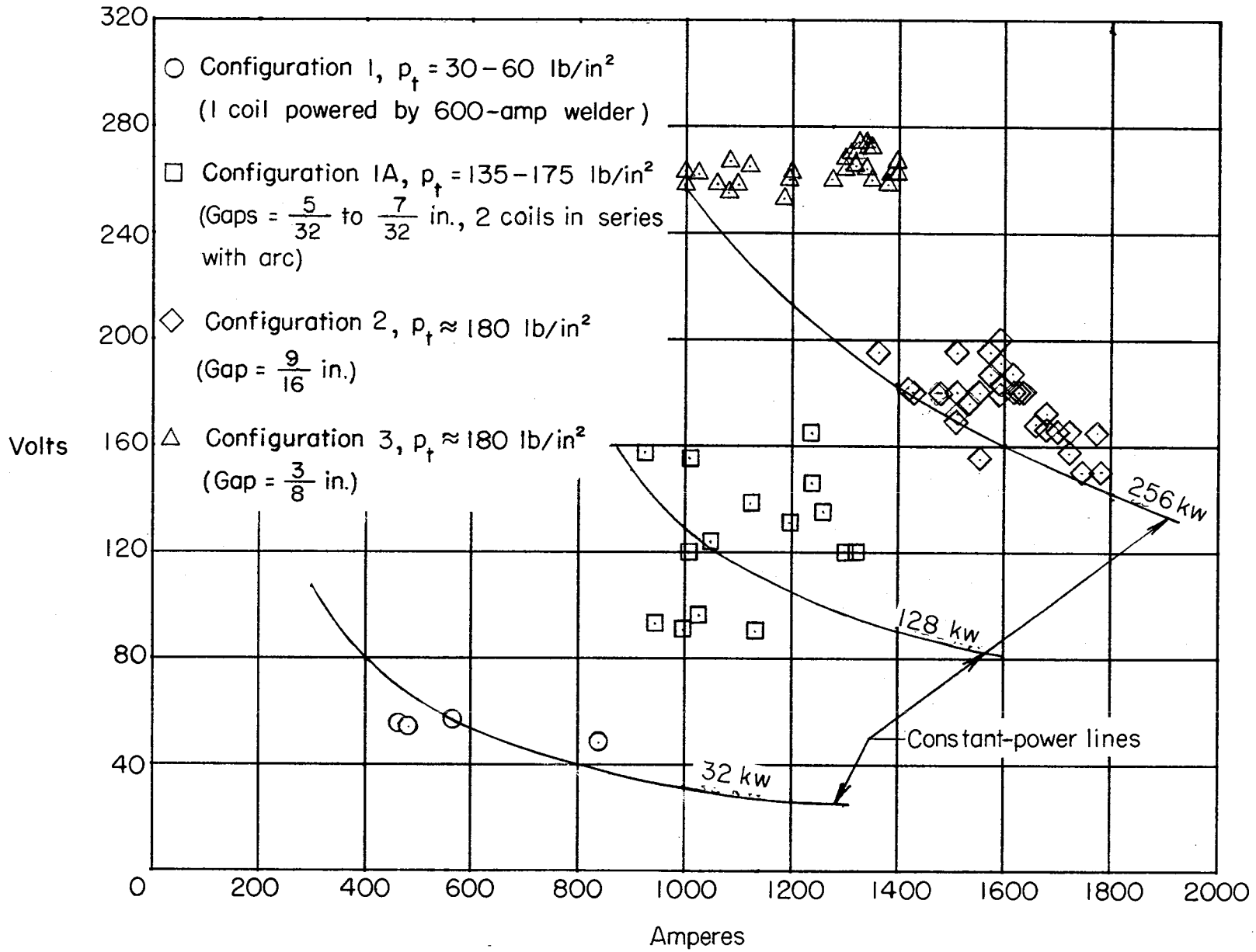

Figure 5.- Arc characteristic measurements with various arc-heater configurations.

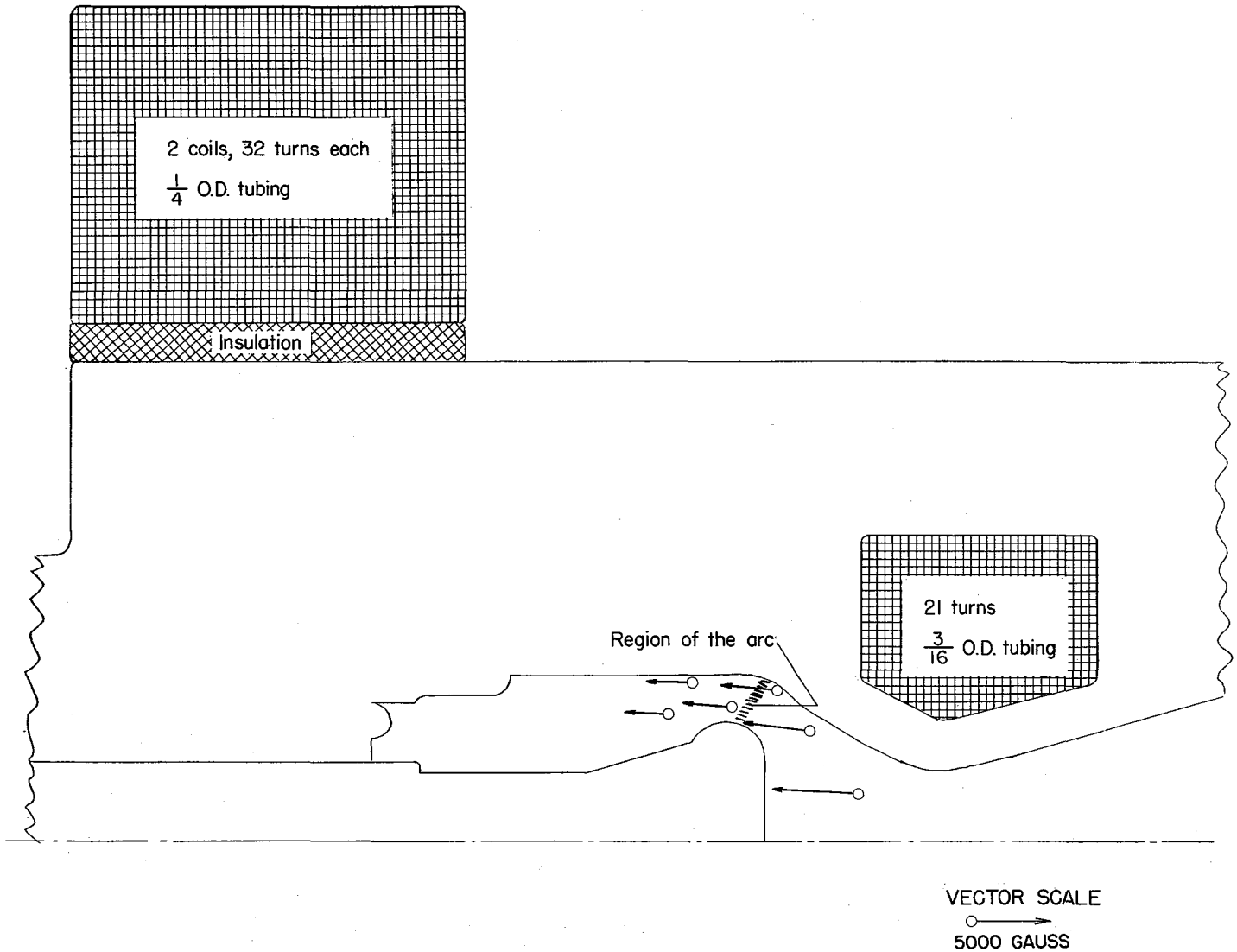

Figure 6.- Simplified cross-sectional view of arc-chamber configuration 2 showing coil locations and the calculated magnetic-field intensity and direction in the region of the arc for 1,600 amperes through the small coil and 800 amperes through each 32-turn section of the large coil.

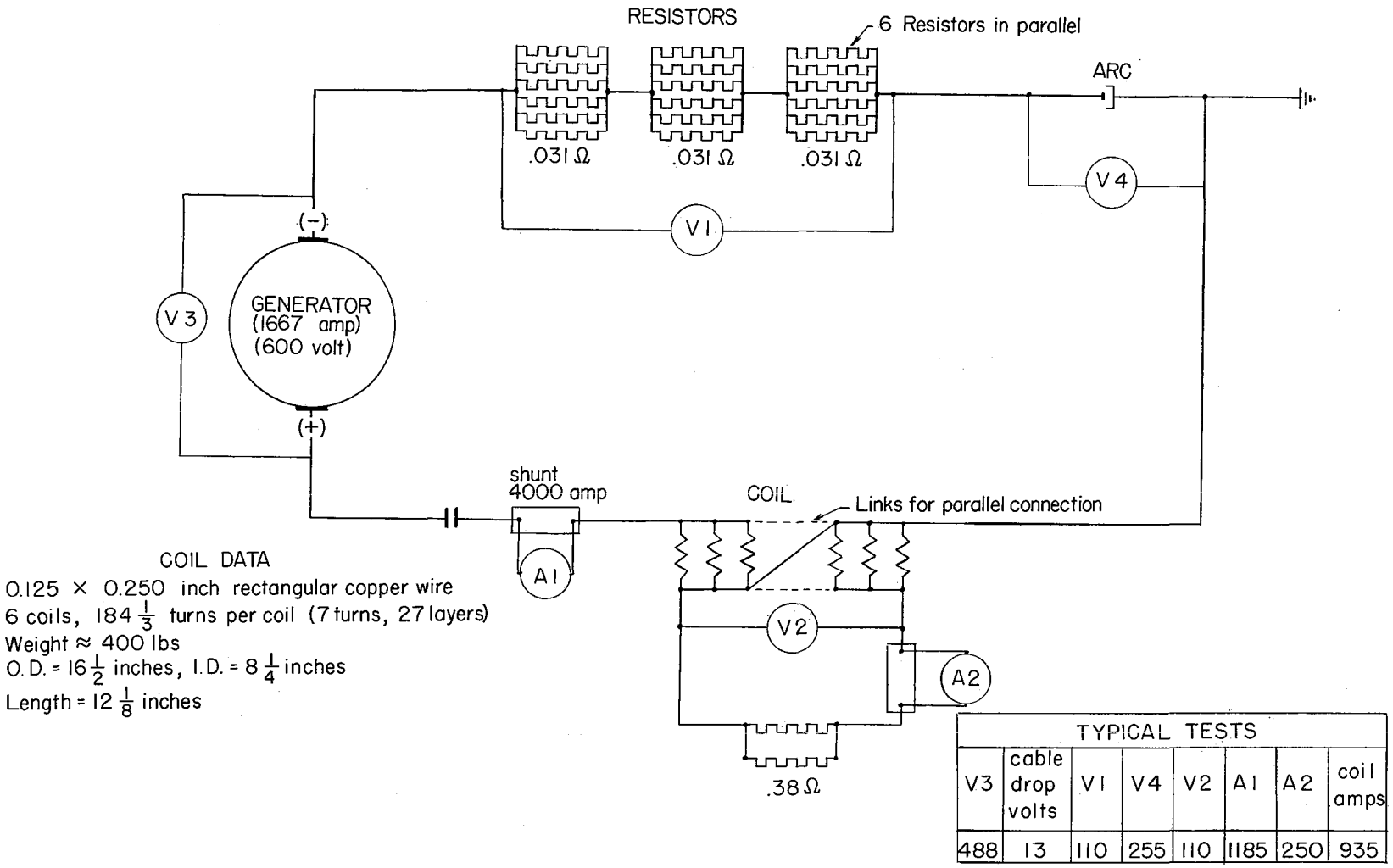

TYPICAL TESTS

V3	cable drop volts	V1	V4	V2	A1	A2	coil amps
488	13	110	255	110	1185	250	935

Figure 7.- Electrical circuit used with configuration 3 showing typical measurements made throughout the circuit. (V denotes voltmeter; A denotes ammeter.)

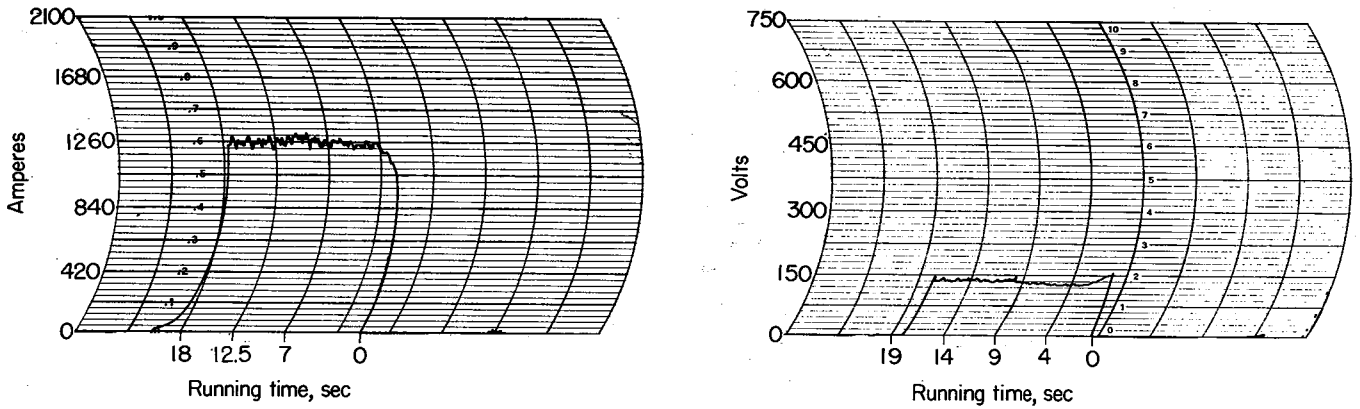

(a) Configuration 2 (approximately 4,000-gauss magnetic field).

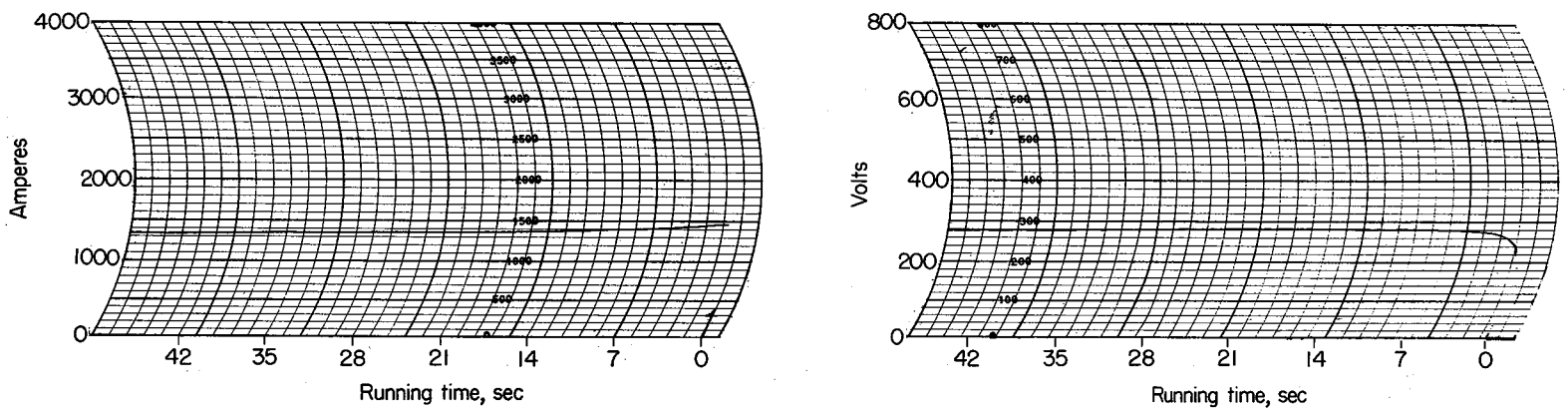

(b) Configuration 3 (approximately 12,000-gauss magnetic field).

Figure 8.- Voltage and amperage traces of a typical test.

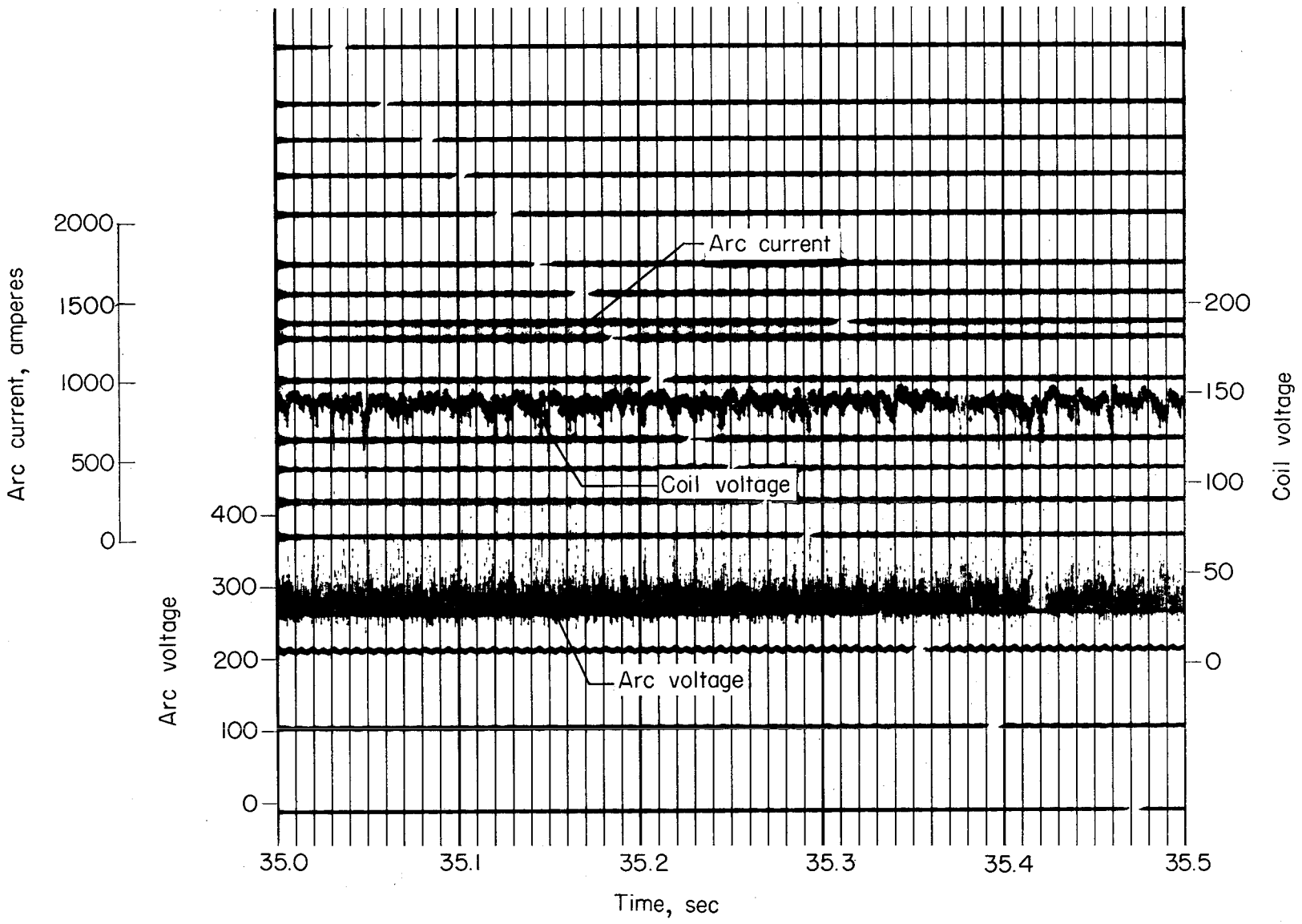

(c) Oscillograph record of test with configuration 3 (approximately 12,000-gauss magnetic field).

Figure 8.- Concluded.

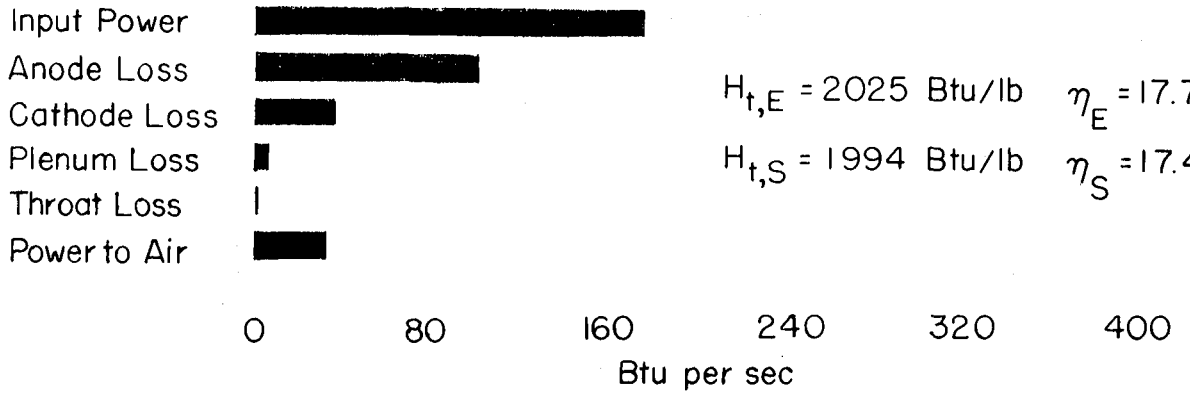

(a) Configuration 1A, p_t = 11.2 atmospheres, $\dot{m}$ = 0.0151 lb/sec.

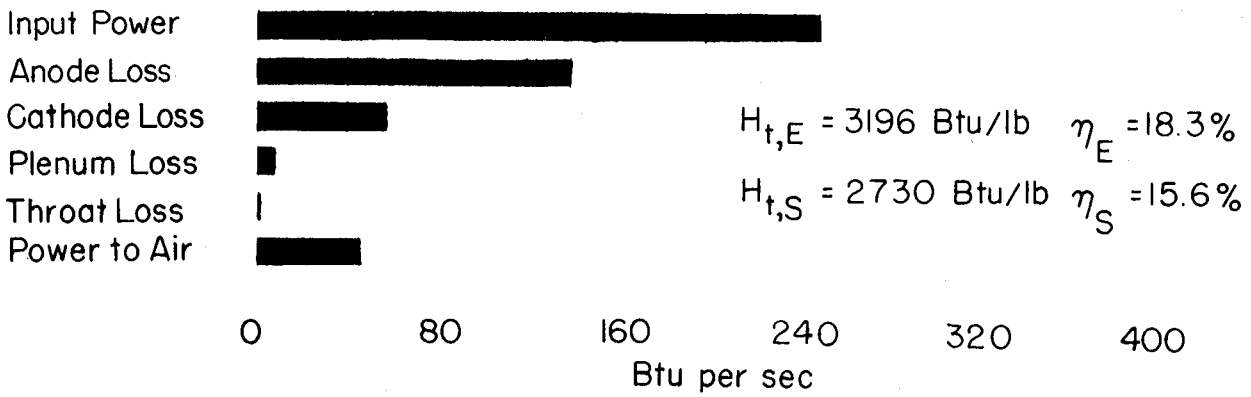

(b) Configuration 2, p_t = 12.36 atmospheres, $\dot{m}$ = 0.0144 lb/sec.

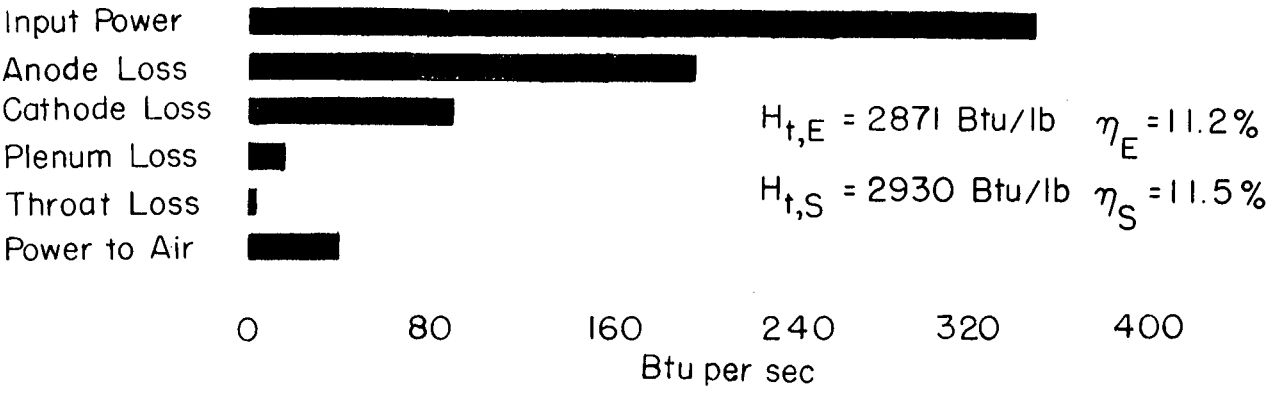

(c) Configuration 3, p_t = 12.15 atmospheres, $\dot{m}$ = 0.0137 lb/sec.

Figure 9.- Bar graphs of arc-heater performance. Cross-hatched portions represent calculated power in air at a location just upstream of throat section.

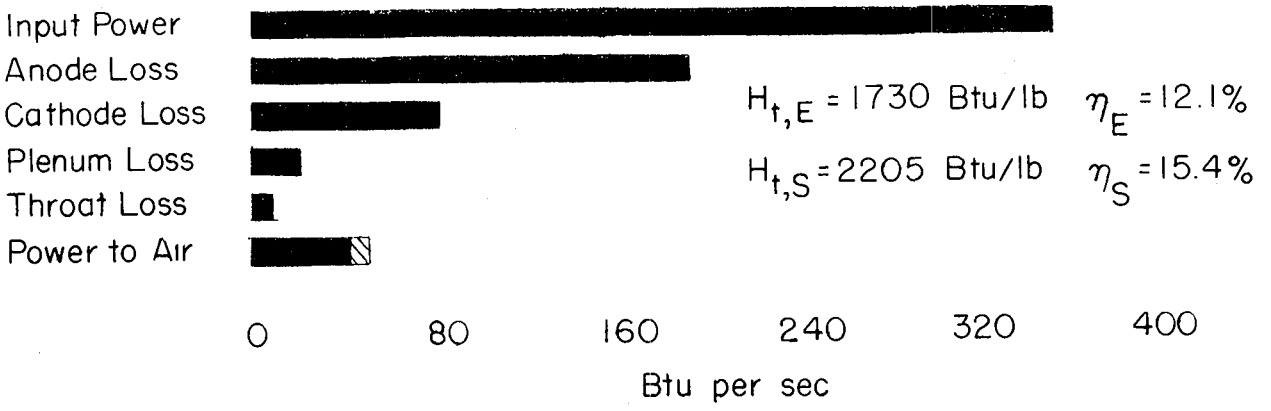

(d) Configuration 3, p_t = 19.45 atmospheres, $\dot{m}$ = 0.025 lb/sec.

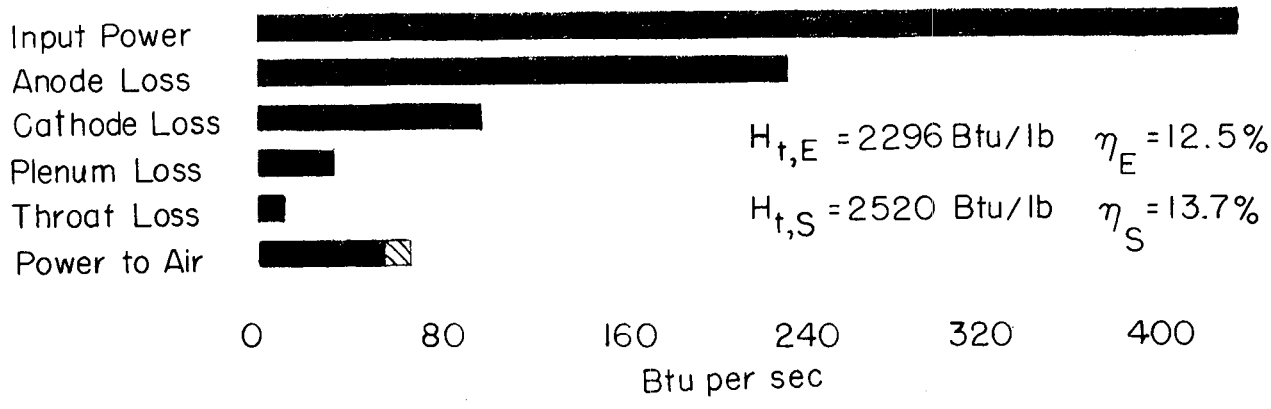

(e) Configuration 3A, p_t = 19.85 atmospheres, $\dot{m}$ = 0.024 lb/sec.

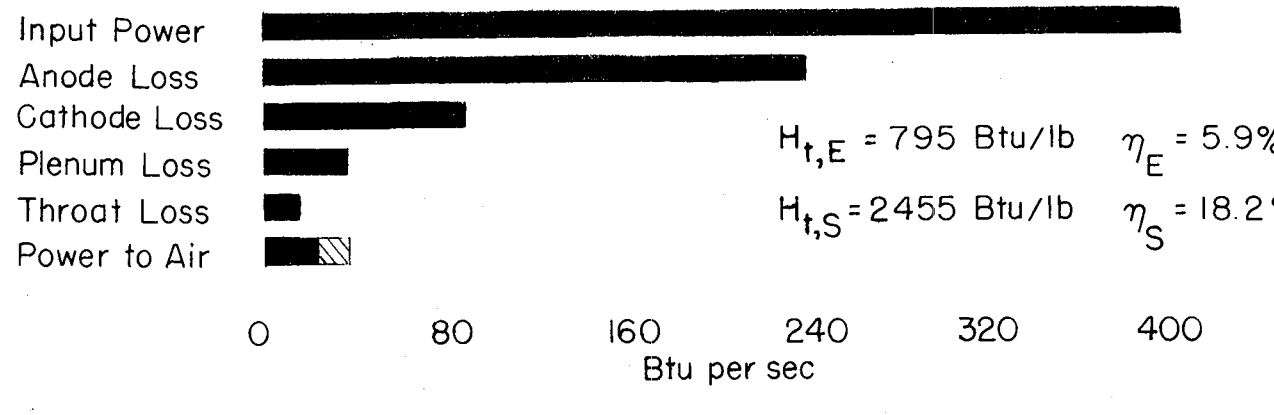

(f) Configuration 3A, p_t = 28.25 atmospheres, $\dot{m}$ = 0.030 lb/sec.

Figure 9.- Concluded.

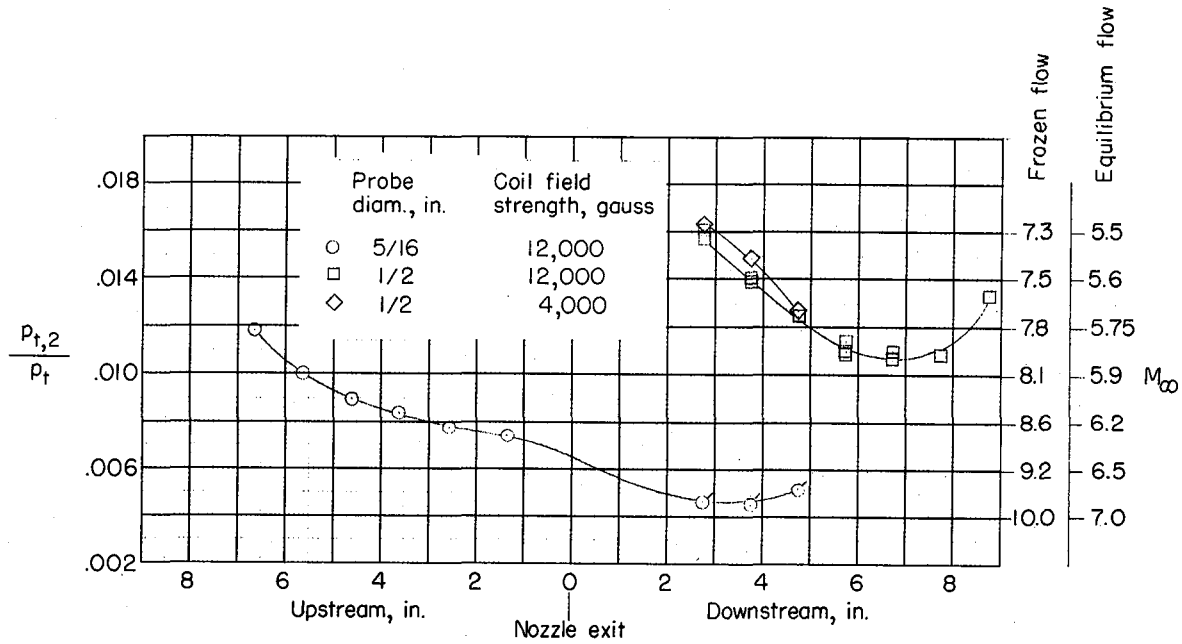

(a) Longitudinal survey along tunnel centerline.

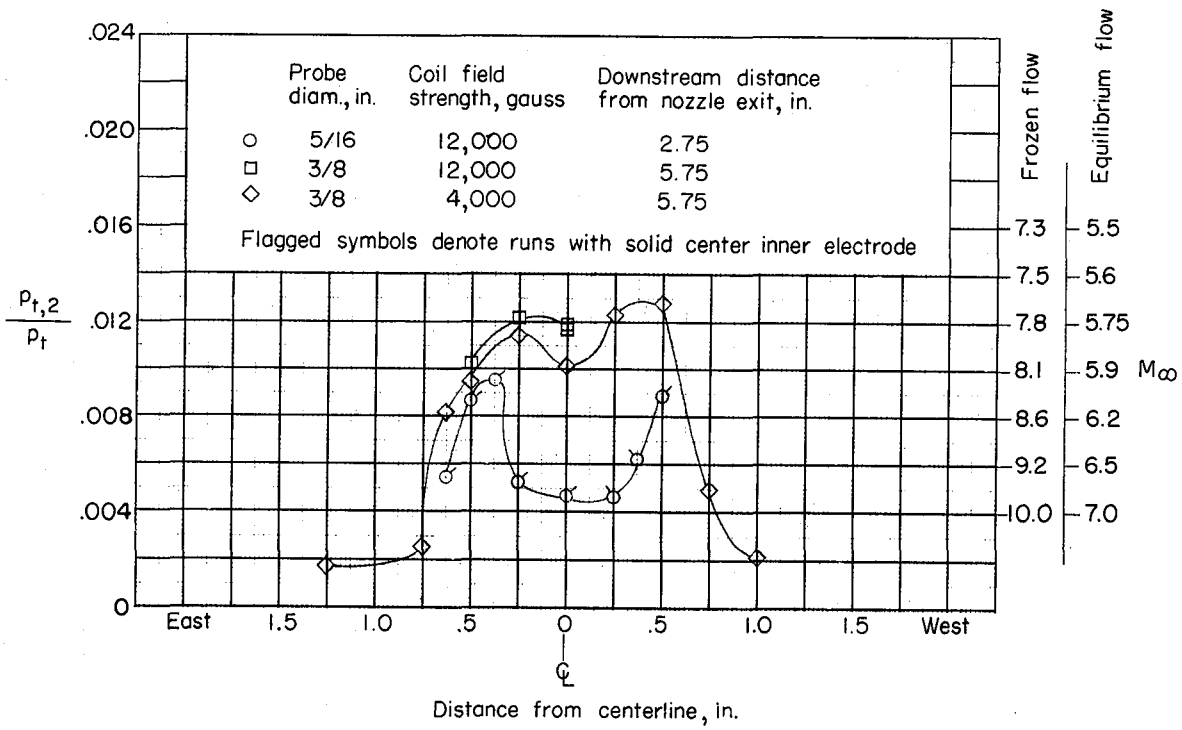

(b) Transverse survey across stream at a station 2.75 inches downstream of nozzle exit.

Figure 10.- Pitot-pressure survey.

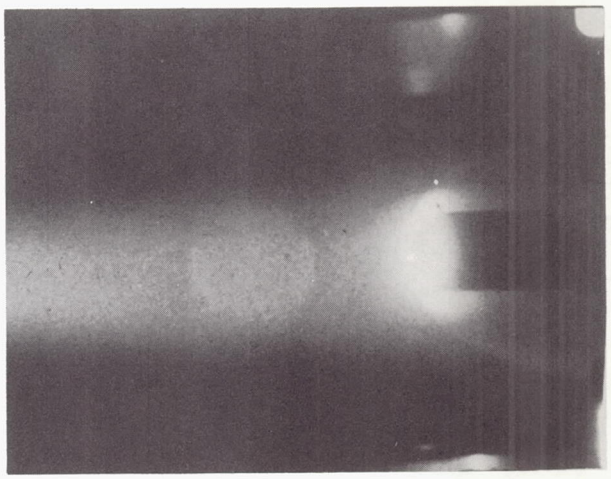

(a) 1/2-inch-diameter, flat-faced tube; arc-heater configuration 2.

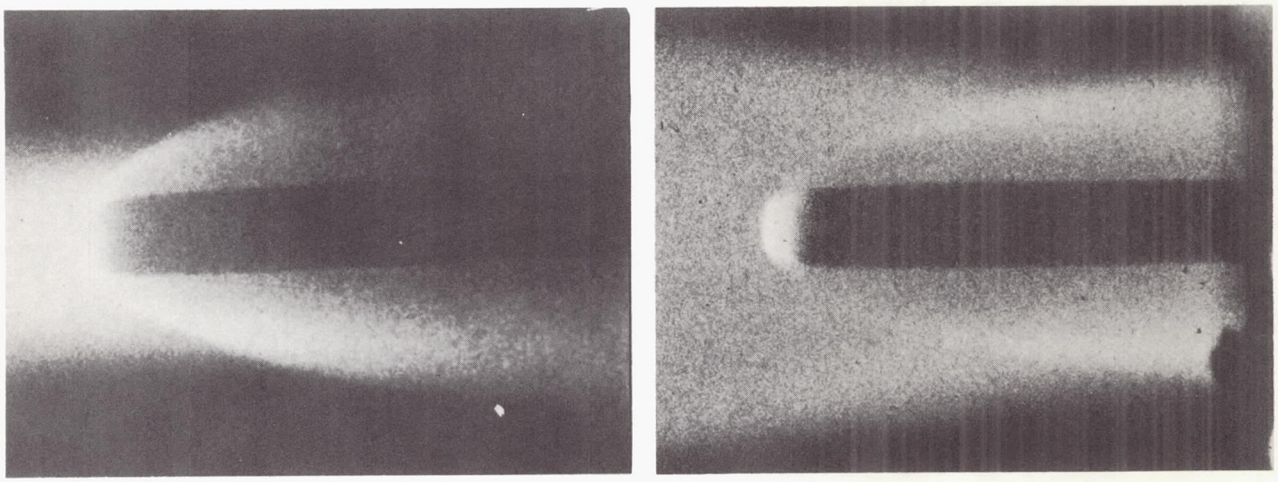

L-62-2126

(b) 5/16-inch-diameter slightly rounded tube; arc-heater configuration 3.

Figure 11.- Photograph of hot gas cap around pitot tubes.

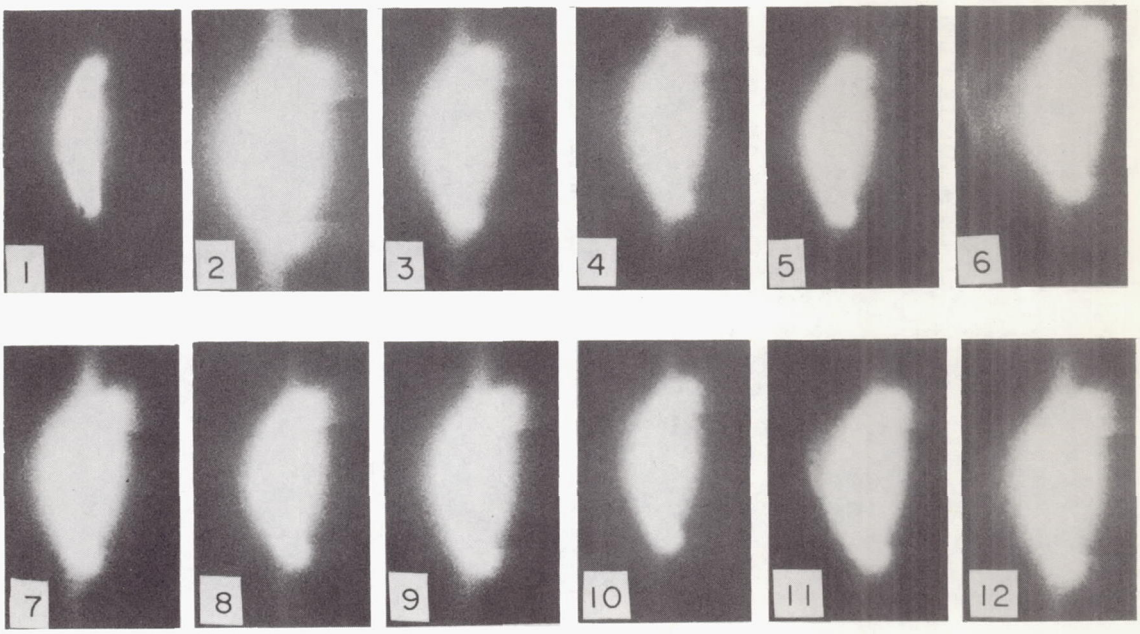

(a) Configuration 2 (4,000-gauss field, p_t = 12.2 atmospheres, T_t = 4,140° K).

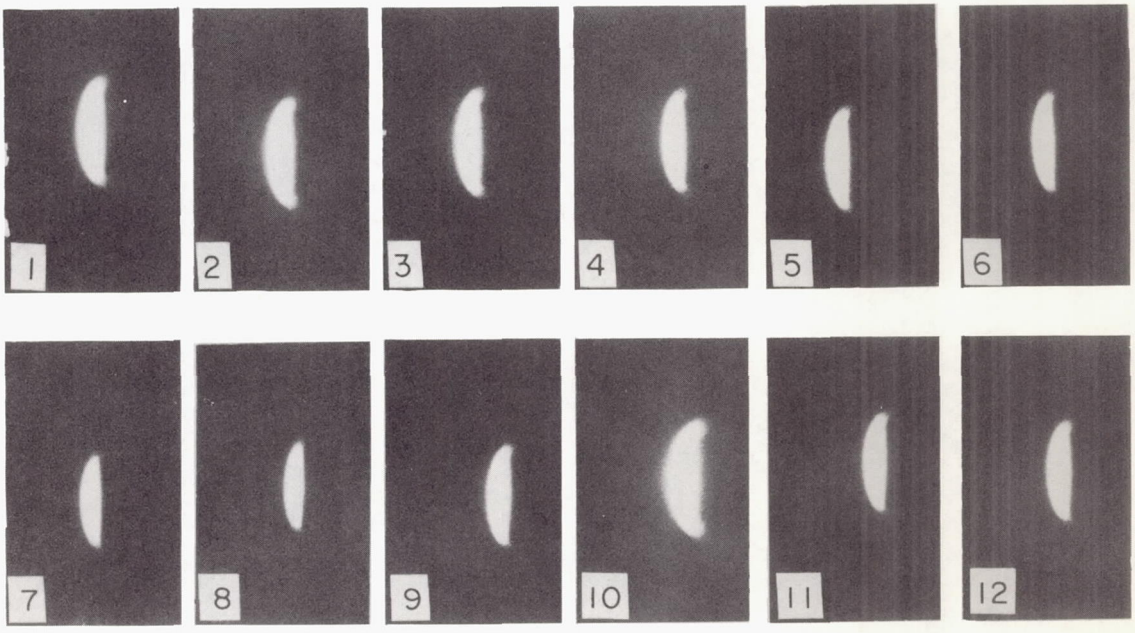

L-62-2127

(b) Configuration 3 (12,000-gauss field, p_t = 12.16 atmospheres, T_t = 3,920° K).

Figure 12.- Successive frames of a high-speed movie (200 frames per second) showing variation in luminosity of the hot gas cap at the nose of a 1/2-inch-diameter flat-faced water-cooled pitot tube.

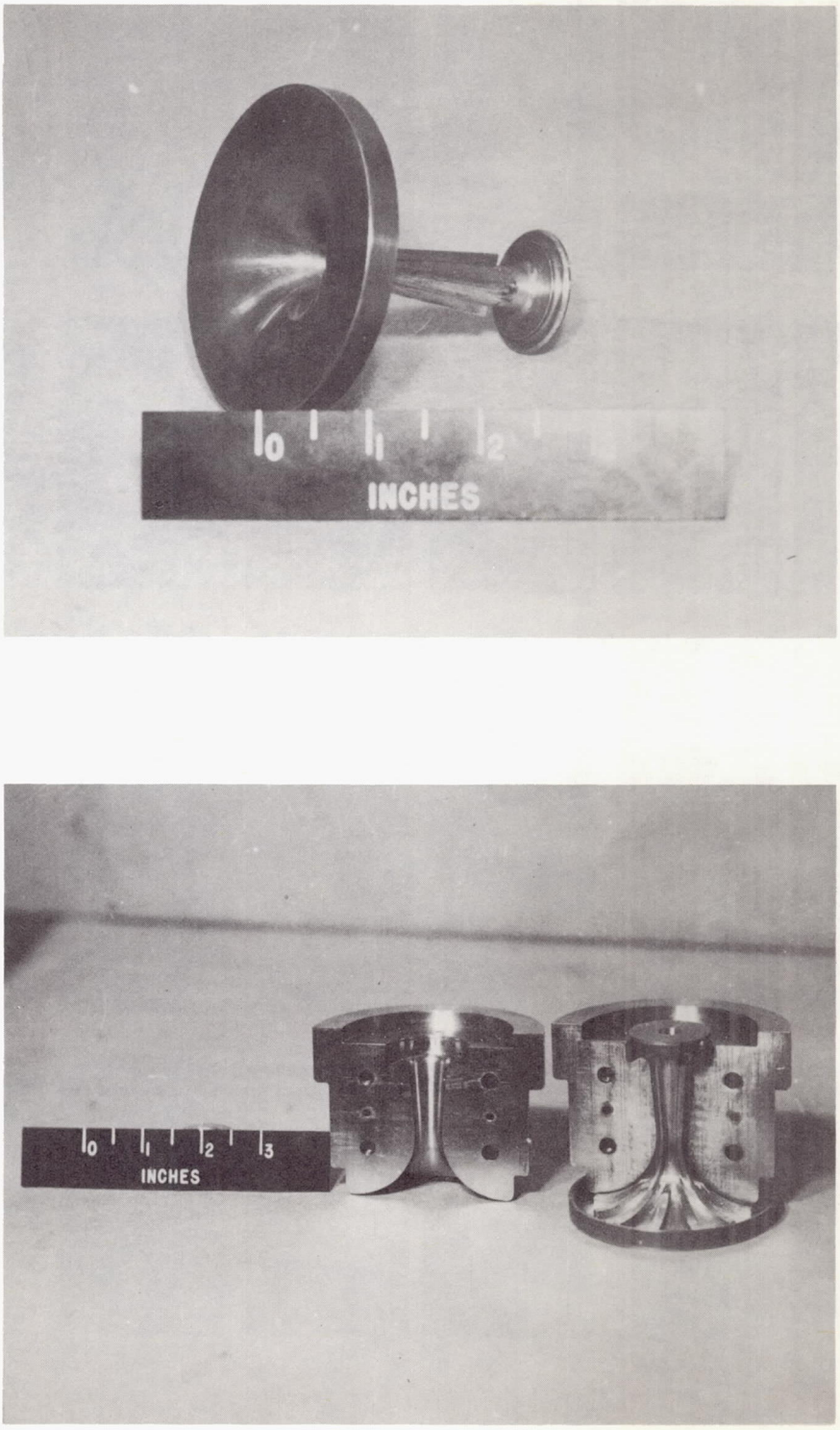

L-62-2128

Figure 13.- Photographs of splined copper throat liner and split housing.

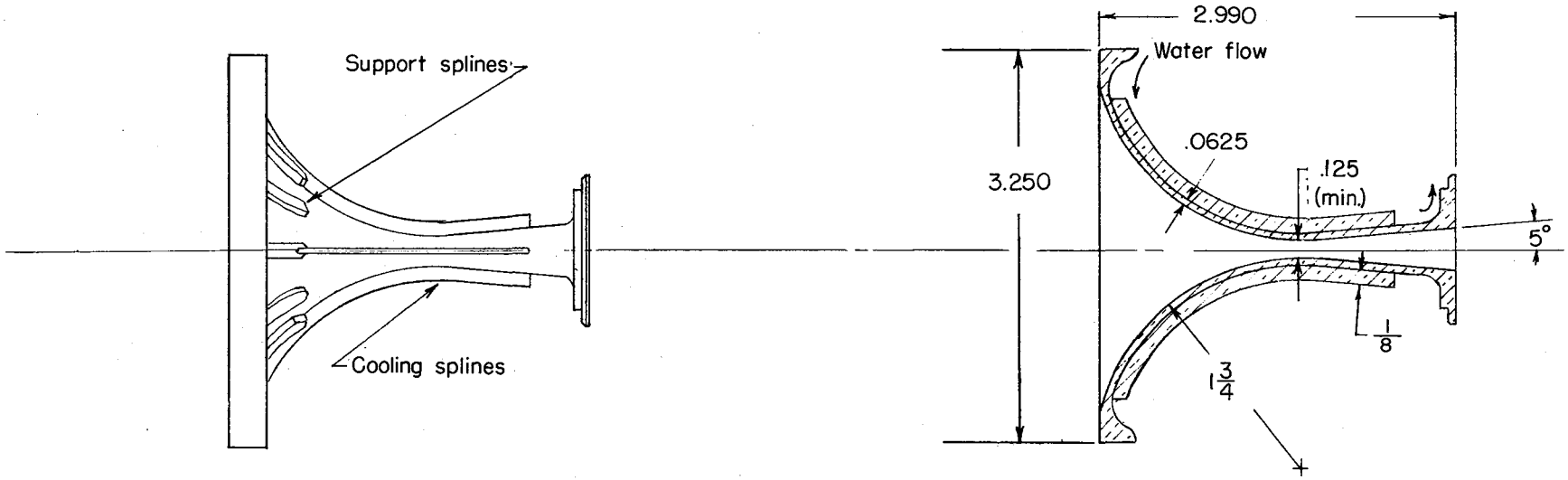

(a) Splined copper throat liner.

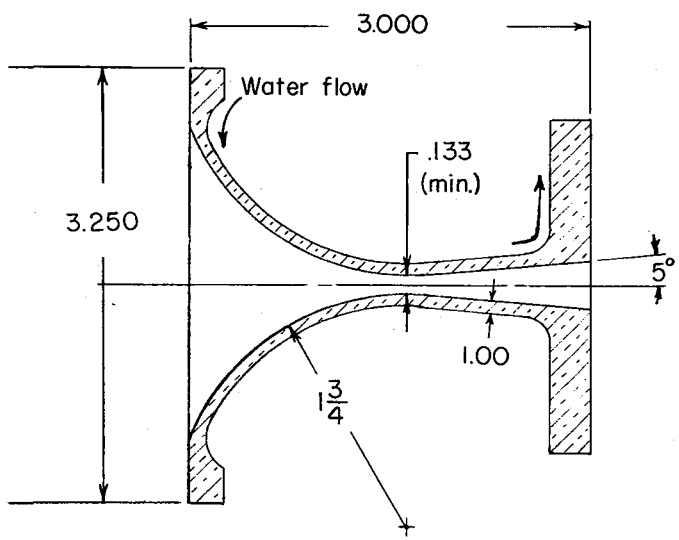

(b) Beryllium copper throat liner.

Figure 14.- Sketches of throat liners. (All dimensions are in inches.)

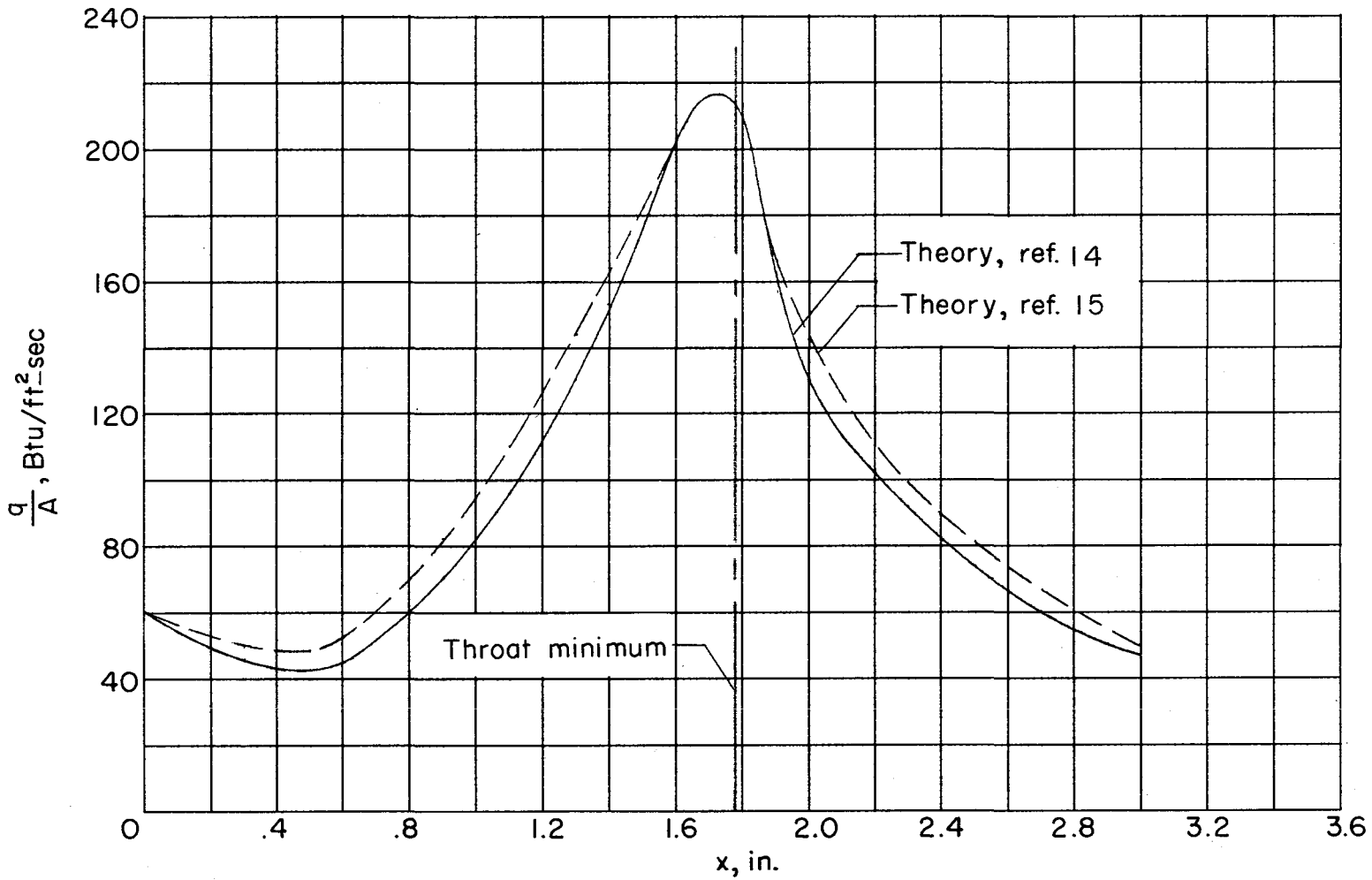

Figure 15.- Calculated heating rates along throat section. T_t = 4,000° K; p_t = 12 atmospheres.

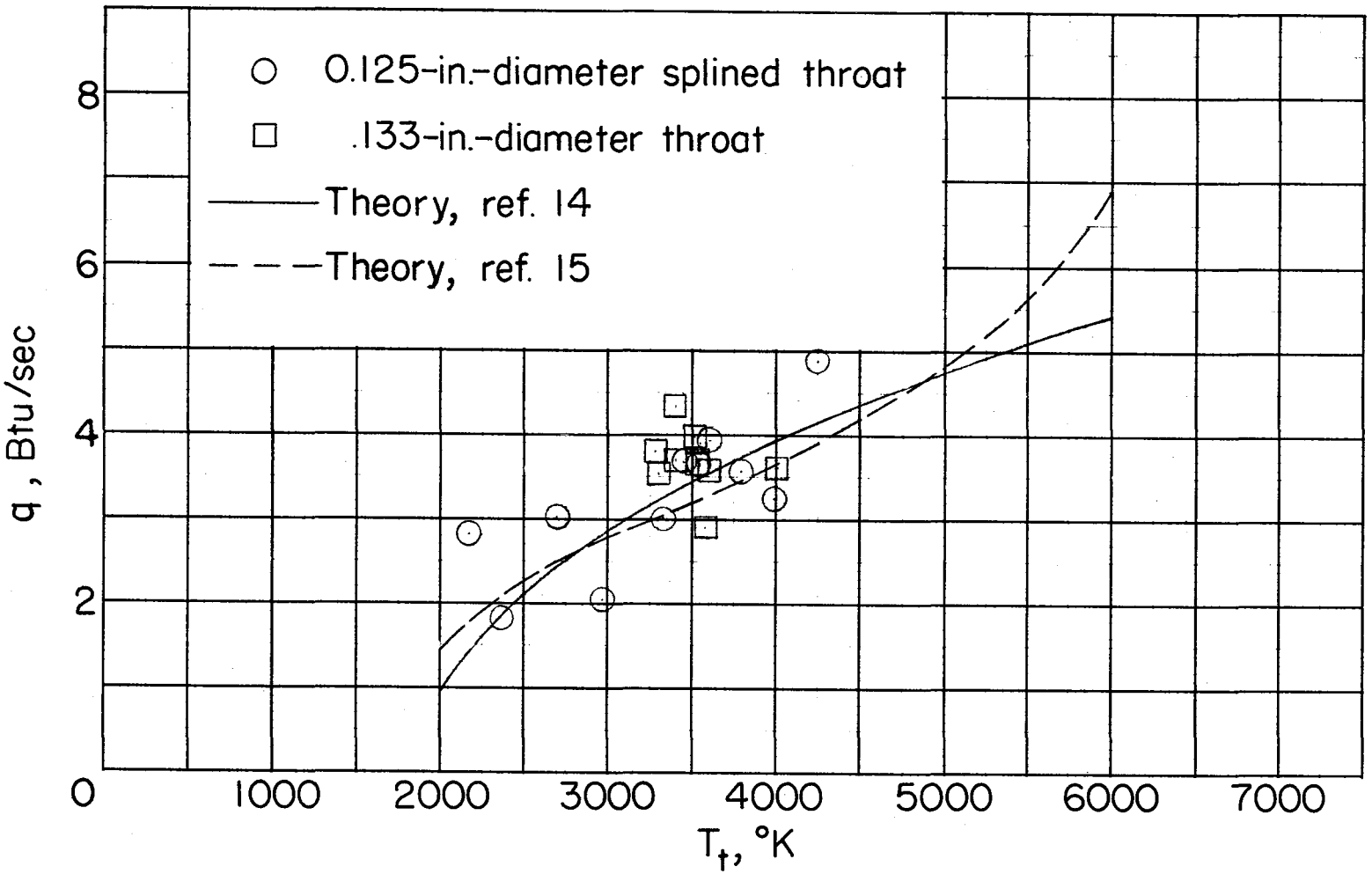

Figure 16.- Measured and predicted total-heat load to throat section.